The Final Report

Title: Numerical Investigation for Microstructural Effects on the Crack Growth Behavior of Particulate Composite Materials

Principal Investigator:
Hiroshi Okada, Ph.D., Associate Professor
Department of Nano Structure and Advanced Materials
Graduate School of Science and Engineering, Kagoshima University
1-21-40 Korimoto, Kagoshima 890-0065, Japan
Telephone, Facsimile: +81-99-285-8249, +81-99-250-3181
E-mail: okada@mech.kagoshima-u.ac.jp

Contract Number: FA520904P0397

AOARD Reference Number: AOARD-044-047

AOARD Program Manager: Tae-Woo Park, Ph.D.

Period of Performance: 23 June 2004 – 22 June 2006

Submission Date: 26 July 2006

Report Documentation Page

Form Approved
OMB No. 0704-0188

1. REPORT DATE	2. REPORT TYPE	3. DATES COVERED
02 AUG 2006	**Final Report (Technical)**	**23-06-2004 to 22-06-2006**

4. TITLE AND SUBTITLE
Numerical Investigation for the Microstructural Effects on the Crack Growth Behavior of Particulate Composite Materials

5a. CONTRACT NUMBER
FA520904P0397

5b. GRANT NUMBER

5c. PROGRAM ELEMENT NUMBER

6. AUTHOR(S)
Hiroshi Okada

5d. PROJECT NUMBER

5e. TASK NUMBER

5f. WORK UNIT NUMBER

7. PERFORMING ORGANIZATION NAME(S) AND ADDRESS(ES)
Kagoshima University,1-21-40 Korimoto,Kagoshima 890-0065, ,Japan,JP,890-0065

8. PERFORMING ORGANIZATION REPORT NUMBER
AOARD-044047

9. SPONSORING/MONITORING AGENCY NAME(S) AND ADDRESS(ES)
The US Resarch Labolatory, AOARD/AFOSR, Unit 45002, APO, AP, 96337-5002

10. SPONSOR/MONITOR'S ACRONYM(S)
AOARD/AFOSR

11. SPONSOR/MONITOR'S REPORT NUMBER(S)

12. DISTRIBUTION/AVAILABILITY STATEMENT
Approved for public release; distribution unlimited

13. SUPPLEMENTARY NOTES

14. ABSTRACT
In present investigation, analyses for the damage evolution behavior of particulate composite materials by using the finite element method (FEM) and the s-version finite element method (s-FEM) were carried out. The analyses were carried out in particular interest in the phenomenon of crack propagation. Prior to crack propagation, material damage develops in the material. The material damage may be in the forms of microviod and/or microcracks in the binder (matrix) and in the form of binder (matrix)/particle separation that is known to be dewetting. In a macroscopic sense, the reinforcing particles distribute evenly in matrix. However, at microscopic level, the density of the distributed particles varies. This means that the stiffness and strength of the material also have some spatial variations. Material damages initiate at the weak material locations and then propagate the surroundings. When cracks are present in the material, the cracks interact with the surroundings and the material To simulate such scenarios, we adopted two kinds of damage constitutive models. One is isotropic damage model and the other is ?separate dilatational/deviatoric damage constitutive model? in which the contributions of hydrostatic and of deviatoric stresses are accounted for independently. A parameter in the separate dilatational/ deviatoric damage model can characterize which, hydrostatic or deviatoric stress component, has dominant influence to the damage behavior of the material. A series of analyses on uncracked and cracked specimen with statistically varying material stiffness at a microscopic level were carried out. The results revealed that the damage behavior is highly influenced by the damage mode.

15. SUBJECT TERMS
Fracture Mechanics

16. SECURITY CLASSIFICATION OF:			17. LIMITATION OF ABSTRACT	18. NUMBER OF PAGES	19a. NAME OF RESPONSIBLE PERSON
a. REPORT **unclassified**	b. ABSTRACT **unclassified**	c. THIS PAGE **unclassified**		**62**	

Standard Form 298 (Rev. 8-98)
Prescribed by ANSI Std Z39-18

Final Report

Numerical investigation for microstructural effects on the crack growth behavior of particulate composite materials

P.I.: Hiroshi Okada, Ph.D., Associate Professor

Address: Department of Nano Structure and Advanced Materials
Graduate School of Science and Engineering, Kagoshima University
1-21-40 Korimoto, Kagoshima 890-0065, Japan

Telephone, Facsimile: +81-99-285-8249, +81-99-250-3181
E-mail: okada@mech.kagoshima-u.ac.jp

Contents

Contents……1
Summary……3

1. Damage constitutive law……...4
1.1 Isotropic damage……..4
1.2 Separate Isotropic/deviatoric damage model……6
1.3 Determining damage evolution law for the isotropic damage material……8
1.4 Determining damage evolution law for the separate Isotropic/deviatoric damage model……10

2. Numerical Implementation of the Damage Constitutive Laws in an In-House Finite Element Program……15
2.1 The s-version finite element method (s-FEM)……15
2.2 Incremental algorithm……18
2.3 Some other issues associated with the damage constitutive law-initiation of nonlinear deformation……...19
2.4 Some other issues associated with the damage constitutive law-initiation of nonlinear deformation……...19

3. Numerical demonstrations of s-FEM computer program with the damage constitutive laws……..24
3.1 Stress-strain relationship……24
3.2 Example problem-isotropic damage model……25
3.3 Example problem-separate Isotropic/deviatoric damage model……27
3.4 Summary-Numerical demonstrations on the damage constitutive models and the s-FEM computer program……30

4. Investigating the Effects of Micro-Structure on the Tensile Behavior of a Solid Propellant……31
4.1 The behavior of a tensile block-Isotropic damage constitutive model……33
4.2 The behavior of a tensile block- separate Isotropic/deviatoric damage model..36
4.3 The behavior of a cracked specimen – isotropic damage model……44
4.4 The behavior of a cracked specimen – separate isotropic/deviatoric damage model……48

5. Remarks……54
5.1 Summary of present investigation……54
5.2 Findings from the analyses……55
5.3 Relevance to the case of polymeric particulate composite……56

6. Conclusions……..57

References……58
Publications……59
Acknowledgements……..60

Summary

In present investigation, analyses for the damage evolution behavior of particulate composite materials by using the finite element method (FEM) and the s-version finite element method (s-FEM) were carried out. The analyses were carried out in particular interest in the phenomenon of crack propagation.

Prior to crack propagation, material damage develops in the material. The material damage may be in the forms of microviod and/or microcracks in the binder (matrix) and in the form of binder (matrix)/particle separation that is known to be dewetting. In a macroscopic sense, the reinforcing particles distribute evenly in matrix. However, at microscopic level, the density of the distributed particles varies. This means that the stiffness and strength of the material also have some spatial variations. Material damages initiate at the weak material locations and then propagate the surroundings. When cracks are present in the material, the cracks interact with the surroundings and the material

To simulate such scenarios, we adopted two kinds of damage constitutive models. One is isotropic damage model and the other is “separate dilatational/deviatoric damage constitutive model” in which the contributions of hydrostatic and of deviatoric stresses are accounted for independently. A parameter in the separate dilatational/deviatoric damage model can characterize which, hydrostatic or deviatoric stress component, has dominant influence to the damage behavior of the material.

A series of analyses on uncracked and cracked specimen with statistically varying material stiffness at a microscopic level were carried out. The results revealed that the damage behavior is highly influenced by the damage mode.

1. Damage constitutive law

In present investigation, we adopt the continuum damage constitutive law of Simo and Ju [1, 2]. The damage model was extended so that it can model the isotropic, deviatoric, dilatational and deviatoric/dilatational combined damages was adopted. The constitutive model was implemented in the in-house s-FEM computer program. The s-FEM computer program of Okada et al. [3] can model particulate composite materials by superposing the finite element models for the particles on that for the global structure or for the region of unit cell. A finite element model for a particle and its surrounding material region needs to be built only once. Such finite element model is called the "local model". Then it is repeatedly superposed on the one that represents the global structure, that is called the "global model".

In present investigation, an ordinary finite element method is mostly used. The s-FEM computer program can also be used to carry out ordinary finite element analyses. To do so, we simply do not superpose any local finite element models on the global one.

In this chapter, we first explore the damage constitutive model that is adopted in this research.

1.1 Isotropic damage

First, we describe the isotropic damage theory by following Simo and Ju [1]. In Simo and Ju [1], the effective stress concept and the hypothesis of strain equivalence are described. When they are applied to the case of elastic damage, the elastic potential energy of damaged material, in terms of the strains ε_{ij} and the damage parameter d is written to be:

$$\psi(\varepsilon_{k\ell}, d) = (1-d)\psi^{o}(\varepsilon_{k\ell}) \tag{1}$$

where $\psi^{o}(\varepsilon_{k\ell})$ is the elastic-potential function for virgin material that is written to be:

$$\psi^{o}(\varepsilon_{k\ell}) = \frac{1}{2} C_{ijk\ell}\varepsilon_{ij}\varepsilon_{k\ell} \tag{2}$$

Just like equivalent stress concept in the theory of plasticity, a scalar parameter $\bar{\tau}$ that

measures the magnitude of stress/deformation is introduced.

$$\bar{\tau} = \sqrt{2\psi^{o}(\varepsilon_{k\ell})} \tag{3}$$

Criteria for the damage evolution are written as follows. First, the effective stress needs to reach the critical value.

$$g(\bar{\tau}(\varepsilon_{k\ell}) - r(d)) = \bar{\tau}(\varepsilon_{k\ell}) - r(d) = 0 \tag{4}$$

where $r(d)$ is the function of the damage parameter d. The relationship between $r(d)$ and d needs to be determined based an experimental data. The material damage progresses when the damage parameter increases. Therefore, when the damage is ongoing, the time derivative of the damage parameter $\dot{d}$ must be positive.

$$\dot{d} > 0 \tag{5}$$

$\dot{d}$ is determined through the evolution law, as:

$$\dot{d} = \dot{r}H(\bar{\tau}, d) = \dot{\tau}(\varepsilon_{k\ell})H(\bar{\tau}, d) \tag{6}$$

The constant $H(\bar{\tau}, d)$ characterizes the progress of damage with respect to the effective stress like term. Equations (4) and (5) must be satisfied when the progressive damage takes place. It is noted that the constant $H(\bar{\tau}, d)$ is always positive. Therefore, the equivalent stress-like term must increase to satisfy equation (6), while the material damage is in progress.

Since the elastic potential energy is assumed in the form of equation (1), the stresses σ_{ij} are written in the following form.

$$\sigma_{ij} = (1 - d)C_{ijk\ell}\varepsilon_{k\ell} \tag{7}$$

The rates of stresses can be expressed by differentiating both the sides of equation (7), as:

$$\dot{\sigma}_{ij} = (1-d)C_{ijk\ell}\dot{\varepsilon}_{k\ell} - \dot{d}C_{ijk\ell}\varepsilon_{k\ell} = (1-d)C_{ijk\ell}\dot{\varepsilon}_{k\ell} - \dot{d}\sigma^{o}_{ij} \tag{8}$$

where $\sigma^{o}_{ij}\left(= C_{ijk\ell}\varepsilon_{k\ell}\right)$ are the stresses when the virgin material is assumed for the same strains. From equation (6), the rate $\dot{d}$ of damage parameter d can be derived to be:

$$\dot{d} = \dot{\bar{\tau}}H(\bar{\tau},d) = H(\bar{\tau},d)\frac{\sigma^{o}_{k\ell}}{\bar{\tau}}\dot{\varepsilon}_{k\ell} = \frac{H(\bar{\tau},d)}{\bar{\tau}}\sigma^{o}_{k\ell}\dot{\varepsilon}_{k\ell} \tag{9}$$

$H(\bar{\tau},d)$ characterizes the rate of damage parameter d with respect to the rate of the effective stress-like parameter $\dot{\bar{\tau}}$.
Substituting equation (9) in equation (8), we arrive at:

$$\begin{aligned}\dot{\sigma}_{ij} &= (1-d)C_{ijk\ell}\dot{\varepsilon}_{k\ell} - \dot{d}\sigma^{o}_{ij} = (1-d)C_{ijk\ell}\dot{\varepsilon}_{k\ell} - \frac{H(\bar{\tau},d)}{\bar{\tau}}\sigma^{o}_{ij}\sigma^{o}_{k\ell}\dot{\varepsilon}_{k\ell} \\ &= D^{ID}_{ijk\ell}\dot{\varepsilon}_{k\ell}\end{aligned} \tag{10}$$

where

$$D^{ID}_{ijk\ell} = (1-d)C_{ijk\ell} - \frac{H(\bar{\tau},d)}{\bar{\tau}}\sigma^{o}_{ij}\sigma^{o}_{k\ell} \tag{11}$$

$D^{ID}_{ijk\ell}$ are the tangent moduli for the isotropic damage material and have the major and minor symmetries, i.e. $D^{ID}_{ijk\ell} = D^{ID}_{k\ell ij}$, $D^{ID}_{ijk\ell} = D^{ID}_{ij\ell k}$ and $D^{ID}_{ijk\ell} = D^{ID}_{jik\ell}$.

1.2 Separate Isotropic/deviatoric damage model

The damage evolution of some class of materials are more sensitive to hydrostatic pressure stress than shear stresses. A typical scenario is in a material containing microvoids. Microvoids grow under applied positive-hydrostatic pressure stress. But they do not grow under negative-hydrostatic pressure stress. The growths of the voids are assumed to be less sensitive to the shear (deviatoric) stresses than positive-hydrostatic stress.

One way to model such material is to separate the contributions of hydrostatic and deviatoric stresses to the damage growth. To do so with a very simple model, we separate the damage parameter d into the dilatational (volumetric) and deviatoric parts. Hence, the elastic potential energy function [equation (1)] is modified and is written to be:

$$\psi(\varepsilon_{k\ell}, d_V, d_D) = (1-d_V)\psi_V^o(\varepsilon_{kk}) + (1-d_D)\psi_D^o(\varepsilon'_{ij}) \tag{12}$$

where ε_{kk} and ε'_{ij} are the volumetric and deviatoric strains. The functions ψ_V^o and ψ_D^o are defined to be:

$$\psi_V^o = \frac{1}{2}K(\varepsilon_{kk})^2 \quad \text{and} \quad \psi_V^o = \mu\varepsilon'_{ij}\varepsilon'_{ij} \tag{13}$$

where K and μ are the bulk and shear moduli. It is noted here that under a constraint condition $d_V = d_D$, the separate dilatational/deviatoric damage model is the same as the isotropic damage model. We define two kinds of effective stress-like terms, as:

$$\bar{\tau}_V = \sqrt{2\psi_V^o(\varepsilon_{kk})} = \sqrt{K(\varepsilon_{kk})^2} \quad \text{and} \quad \bar{\tau}_D = \sqrt{2\psi_D^o(\varepsilon'_{ij})} = \sqrt{2\mu\varepsilon'_{ij}\varepsilon'} \tag{14}$$

When the damages are in progress, the following conditions must be satisfied.

$$\bar{\tau}_V = r_v(d_v) \quad \text{and} \quad \sigma_{kk} > 0 \quad \text{for the dilatational damage} \tag{15}$$

$$\bar{\tau}_D = r_v(d_D) \quad \text{for the deviatoric damage} \tag{16}$$

The evolution equations for the damage parameters are written, as:

$$\dot{d}_V = \dot{\bar{\tau}}_V H_V(\bar{\tau}_V, d_V) = H_V(\bar{\tau}_V, d_V)\sqrt{K}\dot{\varepsilon}_{kk} = H_V(\bar{\tau}_V, d_V)\frac{K\varepsilon_{pp}}{\sqrt{K(\varepsilon_{qq})^2}}\dot{\varepsilon}_{kk} \tag{17}$$

$$\dot{d}_D = \dot{\bar{\tau}}_D H_D(\bar{\tau}_D, d_D) = H_D(\bar{\tau}_D, d_D) \frac{2\mu\varepsilon'_{k\ell}}{\sqrt{2\mu\varepsilon'_{pq}\varepsilon'_{pq}}} \varepsilon'_{k\ell} \tag{18}$$

The constants $H_V(\bar{\tau}_V, d_V)$ and $H_D(\bar{\tau}_D, d_D)$ govern the evolution laws for the damage parameters. The constants are the functions of the effective stress-like terms $\bar{\tau}_V$ and $\bar{\tau}_D$ and of the damage parameters d_V and d_D. From equation (12), we can write the stresses, as:

$$\sigma_{ij} = \frac{\partial \psi(\varepsilon_{k\ell}, d_V, d_D)}{\partial \varepsilon_{ij}} = (1 - d_V)\delta_{ij} K \varepsilon_{kk} + 2(1 - d_D)\mu\varepsilon'_{ij} \tag{19}$$

By differentiating both the sides of equation (19) and making use of equations (17) and (18), we can write the rate form constitutive equation, as:

$$\begin{aligned}
\dot{\sigma}_{ij} &= (1 - d_V)\delta_{ij} K \dot{\varepsilon}_{kk} + 2(1 - d_D)\mu\dot{\varepsilon}'_{ij} - \dot{d}_V K \varepsilon_{kk} - 2\dot{d}_D \mu\varepsilon'_{ij} \\
&= (1 - d_V)\delta_{ij} K \dot{\varepsilon}_{kk} + 2(1 - d_D)\mu\dot{\varepsilon}'_{ij} - \delta_{ij} \frac{H_V(\bar{\tau}_V, d_V)}{\bar{\tau}_V} (K\varepsilon_{kk})^2 \dot{\varepsilon}_{\ell\ell} - \frac{4H_D(\bar{\tau}_D, d_D)}{\bar{\tau}_D} \mu^2 \varepsilon'_{ij}\varepsilon'_{k\ell}\dot{\varepsilon}'_{k\ell} \\
&= D^{V-D}_{ijk\ell} \dot{\varepsilon}_{k\ell}
\end{aligned} \tag{20}$$

and,

$$\begin{aligned}
D^{V-D}_{ijk\ell} &= (1 - d_V) K \delta_{ij}\delta_{k\ell} + (1 - d_D)\mu(\delta_{ik}\delta_{j\ell} + \delta_{jk}\delta_{i\ell}) \\
&- \frac{H_V(\bar{\tau}_V, d_V)}{\bar{\tau}_V} (K\varepsilon_{kk})^2 \delta_{ij}\delta_{k\ell} - \frac{4H_D(\bar{\tau}_D, d_D)}{\bar{\tau}_D} \mu^2 \varepsilon'_{ij}\varepsilon'_{k\ell}
\end{aligned} \tag{21}$$

$D^{V-D}_{ijk\ell}$ are the tangent moduli that relate the rate of stresses to those of strains. It is noted that $D^{V-D}_{ijk\ell}$ have the major and minor symmetries, i.e. $D^{V-D}_{ijk\ell} = D^{V-D}_{k\ell ij}$, $D^{V-D}_{ijk\ell} = D^{V-D}_{ij\ell k}$ and $D^{V-D}_{ijk\ell} = D^{V-D}_{jik\ell}$.

1.3 Determining damage evolution law for the isotropic damage material

The damage evolution law of equation (9) has a scalar function $H(\bar{\tau}, d)$ of $\bar{\tau}$ and d. $H(\bar{\tau}, d)$ characterizes the damage evolution behavior and should be derived from a set

of experimental data. In this section, how the scalar function $H(\bar{\tau},d)$ is determined is described.

First, we assume that we have a stress-strain curve which was measured in an experiment. Let us assume that we have a uniaxial stress-strain curve, as shown in Figure 1. Stress is written by the following equation:

$$\sigma = (1-d)E\varepsilon \tag{22}$$

Therefore, the damage parameter d is expressed by the stress and strain, as:

$$d = 1 - \frac{\sigma}{E\varepsilon} \tag{23}$$

The value of the effective stress-like parameter $\bar{\tau}$ can be written in terms of the uniaxial stress and strain, as:

$$\bar{\tau} = \sqrt{C_{ijk\ell}\varepsilon_{ij}\varepsilon_{k\ell}} = \sqrt{\sigma^o_{k\ell}\varepsilon_{k\ell}} = \sqrt{\frac{\sigma_{k\ell}}{1-d}\varepsilon_{k\ell}} = \sqrt{\frac{\sigma}{1-d}\varepsilon} = \sqrt{\sigma^o\varepsilon} = \sqrt{E\varepsilon^2} \tag{24}$$

Therefore, once the uniaxial stress-strain curve is given, relationship between the effective stress-like and the damage parameter can be obtained. In present investigation, a uniaxial stress-strain curve is approximated by a series of piecewise straight lines, as depicted in Figure 2. In Figure 2, points on the stress-strain curve (σ_1,ε_1), (σ_2,ε_2), (σ_3,ε_3), $\bullet\bullet\bullet$, (σ_i,ε_i), $(\sigma_{i+1},\varepsilon_{i+1})$, $\bullet\bullet\bullet$ connect straight line segments. From a set of data (σ_1,ε_1), (σ_2,ε_2), (σ_3,ε_3), $\bullet\bullet\bullet$, (σ_i,ε_i), $(\sigma_{i+1},\varepsilon_{i+1})$, $\bullet\bullet\bullet$, we can compute $(\bar{\tau}_1,d_1)$, $(\bar{\tau}_2,d_2)$, $(\bar{\tau}_3,d_3)$, $\bullet\bullet\bullet$, $(\bar{\tau}_i,d_i)$, $(\bar{\tau}_{i+1},d_{i+1})$, $\bullet\bullet\bullet$ by using equations (23) and (24). Thus, the relationship between $\bar{\tau}$ and d is also approximated by a series of piecewise straight lines. The function $H(\bar{\tau},d)$ which governs the damage evolution law of equation (6) is approximated by:

$$H(\bar{\tau},d) = \frac{\dot{d}}{\dot{\bar{\tau}}} \approx \frac{d_{i+1}-d_i}{\bar{\tau}_{i+1}-\bar{\tau}_i} \qquad (d_i < d < d_{i+1}, \bar{\tau}_i < \bar{\tau} < \bar{\tau}_{i+1}) \tag{25}$$

The function $H(\bar{\tau},d)$ whose value is determined by equation (25) is used in the stress-strain relationship of equation (10).

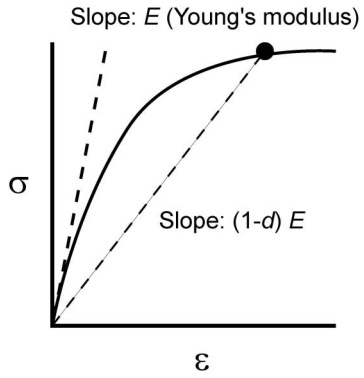

Fig. 1 Uniaxial stress-strain curve

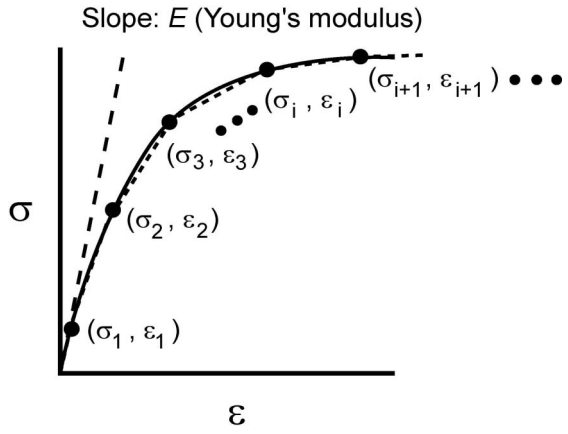

Fig. 2 Piecewise linear approximation for uniaxial stress-strain curve

1.4 Determining damage evolution law for the separate Isotropic/deviatoric damage model

In this section, the damage evolution law for the separate isotropic/deviatoric damage model is dealt with. As seen in equations (17) and (18), there are two different damage evolution laws and two damage variables $H_V(\bar{\tau}_V, d_V)$ and $H_D(\bar{\tau}_D, d_D)$. In order to fully determine $H_V(\bar{\tau}_V, d_V)$ and $H_D(\bar{\tau}_D, d_D)$, we need at least two sets of stress-strain curves. When only one stress-strain curve is available, we need to introduce at least an additional condition. Procedures to determine the damage evolution laws from only one set of uniaxial stress-strain curve are described in this section.

We assume that a uniaxial stress-strain curve, as shown in Figure 1, is available. As an additional condition to uniquely determine the damage evolution law, we postulate that

the ratio (d_V / d_D) between the dilatational and deviatoric damage parameters remains to be the same during the uniaxial deformation. We write:

$$d_D = \alpha d_V \tag{26}$$

Here, α is a positive constant ($0 \le \alpha \le \infty$). When α equals zero, only the dilatational damage is present. When $\alpha = 1$, the magnitudes of dilatational and deviatoric parts equal each other and, therefore, this case is very similar to that of the isotropic damage. When α is infinitely large, the dilatational damage parameter d_V is zero. Therefore, material undergoes deviatoric damage only.

We assume a uniaxial deformation in x_1 direction. We can write the following statements.

$$\begin{aligned} &\sigma_{11} \neq 0 \quad (\text{unknown}); \quad \sigma_{22} = \sigma_{33} = \sigma_{12} = \sigma_{23} = \sigma_{31} = 0 \quad (\text{known}) \\ &\varepsilon_{11} \neq 0, \quad \varepsilon_{12} = \varepsilon_{23} = \varepsilon_{31} = 0 \quad (\text{known}); \quad \varepsilon_{22} = \varepsilon_{33} \quad (\text{unknown}) \end{aligned} \tag{27}$$

Therefore, by substituting equations (26) and (27) in equation (19), we have:

$$\begin{aligned} \sigma_{11} &= (1-d_V)K(\varepsilon_{11}+\varepsilon_{22}+\varepsilon_{33}) + \frac{2}{3}(1-\alpha d_V)\mu(2\varepsilon_{11}-\varepsilon_{22}-\varepsilon_{33}) \\ \sigma_{22} &= (1-d_V)K(\varepsilon_{11}+\varepsilon_{22}+\varepsilon_{33}) + \frac{2}{3}(1-\alpha d_V)\mu(2\varepsilon_{22}-\varepsilon_{33}-\varepsilon_{11}) \\ \sigma_{11} &= (1-d_V)K(\varepsilon_{11}+\varepsilon_{22}+\varepsilon_{33}) + \frac{2}{3}(1-\alpha d_V)\mu(2\varepsilon_{33}-\varepsilon_{11}-\varepsilon_{22}) \end{aligned} \tag{28}$$

From the second and the third of equation (28) and $\varepsilon_{22} = \varepsilon_{33}$, one can obtain:

$$0 = (1-d_V)K(\varepsilon_{11}+\varepsilon_{22}+\varepsilon_{33}) + \frac{2}{3}(1-\alpha d_V)\mu(\varepsilon_{11}-\varepsilon_{22}) \tag{29}$$

The first of equation (28) and equation (29) lead to:

$$\varepsilon_{22} = \frac{-\sigma_{11}}{2(1-\alpha d_V)\mu} + \varepsilon_{11} \tag{30}$$

By substituting equation (30) in the first of equation (28), we can establish a relationship between σ_{11} and ε_{11}, as:

$$3(1-\alpha d_V)(1-d_V)\mu K\varepsilon_{11} - \left\{\frac{1}{3}(1-\alpha d_V)\mu + (1-d_V)K\right\}\sigma_{11} = 0 \tag{31}$$

By rearranging equation (31), we can establish:

$$\alpha d_V^2 + \left\{\frac{\alpha\mu + 3K}{9\mu K}\frac{\sigma_{11}}{\varepsilon_{11}} - (1+\alpha)\right\}d_V + \left(1 - \frac{\sigma_{11}}{E\varepsilon_{11}}\right) = 0 \tag{32}$$

Therefore, for a given set of variables σ_{11}, ε_{11} and α, we can solve for d_V.
Two special cases ($\alpha = 0$ and $\alpha = 1$) are presented first. When $\alpha = 0$, we have:

$$0 \cdot d_V^2 + \left\{\frac{0 \cdot \mu + 3K}{9\mu K}\frac{\sigma_{11}}{\varepsilon_{11}} - (1+0)\right\}d_V + \left(1 - \frac{\sigma_{11}}{E\varepsilon_{11}}\right) = 0 \tag{33}$$

and,

$$d_V = 1 - \frac{\sigma_{11}}{3K\left(3\varepsilon_{11} - \frac{\sigma_{11}}{\mu}\right)} \qquad (\alpha = 0) \tag{34}$$

When $\alpha = 1$, we have:

$$d_V^2 + \left\{\frac{\mu + 3K}{9\mu K}\frac{\sigma_{11}}{\varepsilon_{11}} - 2\right\}d_V + \left(1 - \frac{\sigma_{11}}{E\varepsilon_{11}}\right) = 0 \tag{35}$$

and,

$$d_V = 1 - \frac{\sigma_{11}}{E\varepsilon_{11}} \qquad (\alpha = 0) \tag{36}$$

In is noted that there are two solutions that satisfy equation (35) and they are $d_V = 1 - \frac{\sigma_{11}}{E\varepsilon_{11}}$ and $d_V = 1$. The second one takes a constant value and, therefore, is not a feasible solution. For more general case ($\alpha \neq 0,1$), we solve equation (32) for d_V, by letting:

$$\alpha d_V^2 + Ad_V + B = 0 \tag{37}$$

$$A = \frac{\alpha\mu + 3K}{9\mu K}\frac{\sigma_{11}}{\varepsilon_{11}} - (1+\alpha) \qquad \text{and} \quad B = 1 - \frac{\sigma_{11}}{E\varepsilon_{11}} \tag{38}$$

Therefore, the value d_V is determined to be:

$$d_V = \frac{-A \pm \sqrt{A^2 - 4\alpha B}}{2\alpha} \tag{39}$$

In equation (39), the sign associated with $\sqrt{A^2 - 4\alpha B}$ needs to be determined. To determine the sign, we check a special case ($\alpha = 1$). By letting $\alpha = 1$, in equation (39), we have:

$$d_V = \frac{1}{2}\left\{-\left(\frac{\sigma_{11}}{E\varepsilon_{11}} - 2\right) \pm \frac{\sigma_{11}}{E\varepsilon_{11}}\right\} \tag{40}$$

When we take the positive sign, equation (40) results in:

$$d_V = \frac{1}{2}\left\{-\left(\frac{\sigma_{11}}{E\varepsilon_{11}} - 2\right) + \frac{\sigma_{11}}{E\varepsilon_{11}}\right\} = 1 \tag{41}$$

This is a constant value ($d_V = 1$) and, therefore, is inappropriate. When the negative sign is assumed, we obtain:

$$d_V = \frac{1}{2}\left\{-\left(\frac{\sigma_{11}}{E\varepsilon_{11}} - 2\right) - \frac{\sigma_{11}}{E\varepsilon_{11}}\right\} = 1 - \frac{\sigma_{11}}{E\varepsilon_{11}} \tag{42}$$

This result is the same as the case of isotropic damage material (equation (23)). Therefore, we choose the negative sign in equation (39).

$$d_V = \frac{-A - \sqrt{A^2 - 4\alpha B}}{2\alpha} \tag{43}$$

Thus, the deviatoric damage parameter d_D is also determined to be:

$$d_D = \alpha d_V = \alpha \frac{-A - \sqrt{A^2 - 4\alpha B}}{2\alpha} \tag{44}$$

Once uniaxial stress-strain curve as depicted in Figure 1 is given, we collect a series of points $(\sigma_1, \varepsilon_1)$, $(\sigma_2, \varepsilon_2)$, $(\sigma_3, \varepsilon_3)$, $\bullet\bullet\bullet$, $(\sigma_i, \varepsilon_i)$, $(\sigma_{i+1}, \varepsilon_{i+1})$, $\bullet\bullet\bullet$, on the curve, as shown in Figure 2. Damage parameters ($d_V|_i$ and $d_D|_i$) corresponding to the stress and strain $(\sigma_i, \varepsilon_i)$ are obtained. Thus, by using equations (27) and (28), unknown strains ε_{22} and ε_{33} ($\varepsilon_{22} = \varepsilon_{33}$) are derived. Therefore, we can compute the effective stress-like terms $\bar{\tau}_V \left(= \sqrt{K}\varepsilon_{kk}\right)$ and $\bar{\tau}_D \left(= \sqrt{\mu \varepsilon'_{ij} \varepsilon'_{ij}}\right)$. Thus, we have a series of data $\left(d_V|_1, d_D|_1, \bar{\tau}_V|_1, \bar{\tau}_D|_1\right)$, $\left(d_V|_2, d_D|_2, \bar{\tau}_V|_2, \bar{\tau}_D|_2\right)$, $\left(d_V|_3, d_D|_3, \bar{\tau}_V|_3, \bar{\tau}_D|_3\right)$, $\bullet\bullet\bullet$, $\left(d_V|_i, d_D|_i, \bar{\tau}_V|_i, \bar{\tau}_D|_i\right)$, $\left(d_V|_{i+1}, d_D|_{i+1}, \bar{\tau}_V|_{i+1}, \bar{\tau}_D|_{i+1}\right)$, $\bullet\bullet\bullet$. The scalar functions, $H_V(\bar{\tau}_V, d_V)$ and $H_D(\bar{\tau}_D, d_D)$ are derived to be:

$$\begin{aligned} H_V(\bar{\tau}_V, d_V) &= \frac{\dot{d}_V}{\dot{\bar{\tau}}_V} \approx \frac{d_V|_{i+1} - d_V|_i}{\bar{\tau}_V|_{i+1} - \bar{\tau}_V|_i} \qquad \left(d_V|_i < d_V < d_V|_{i+1}, \bar{\tau}_V|_i < \bar{\tau}_V < \bar{\tau}_V|_{i+1}\right) \\ H_D(\bar{\tau}_D, d_D) &= \frac{\dot{d}_D}{\dot{\bar{\tau}}_D} \approx \frac{d_D|_{i+1} - d_D|_i}{\bar{\tau}_D|_{i+1} - \bar{\tau}_D|_i} \qquad \left(d_D|_i < d_D < d_D|_{i+1}, \bar{\tau}_D|_i < \bar{\tau}_D < \bar{\tau}_D|_{i+1}\right) \end{aligned} \tag{45}$$

2. Numerical Implementation of the Damage Constitutive Laws in an In-House Finite Element Program

The isotropic and the separate isotropic/deviatoric damage models were implemented in an in-house finite element program. In this chapter, the numerical implementations of the damage constitutive laws are described. The in-house finite element program that is used in present investigation is based on the s-version finite element method (s-FEM). In this chapter, (i) the in-house finite element program based on s-FEM, (ii) the implementation of nonlinear constitutive laws in the s-FEM program, (iii) the implementation of isotropic damage constitutive model and (iv) the implementation of isotropic/deviatoric damage model are discussed.

2.1 The s-version finite element method (s-FEM)

In present investigation, the s-FEM program that has been developed in Kagoshima university was adopted as the base program. As described in Okada et al. [3] and Tanaka et al. [4], the s-FEM is the most useful in the analyses of composite material. However, the code can be used as an ordinary finite element program. In this section, the s-FEM for nonlinear analysis is briefly described.

The s-FEM was first proposed by Fish [5] and has been applied to various engineering problems [5,6,7,8]. In the s-FEM, two types of finite element models are used. One is called “global finite element model” or “global model” that covers the whole analysis region. The other is called “local finite element model” or “local model” that is superposed on the global model, as depicted in Figure 3. Typically, the local model has a finer spatial resolution than the global model and is typically placed at the portion of stress concentration, such as crack (see Okada, Endoh and Kikuchi [7]), and second phase material and its vicinity (see Okada et al. [8] and Okada et al. [9]). In Okada et al. [3], an s-FEM formulation that allowed the local models to multiply overlap, as shown in Figure 4.

Let us denote the regions of global model and local models to be Ω^G and Ω^{Li} $(i=1,2,3,\cdots,n)$, respectively. Here, as done in Okada et al. [3], there are many local models that are superposed on the global model and they are allowed to multiply overlap each other. Displacements are expressed by the shape functions of finite elements of global and local models independently. This means that we do not need to

maintain any relationships between the locations of nodes and elements of the global and local models. Therefore, it is quite tractable to enhance the spatial resolution of analysis model locally, by superposing the local models on the global model. It is noted that if there were no overlaid local models, the program performs an ordinary finite element analysis.

When the damage constitutive law is adopted in an analysis, we perform an incremental analysis, just like the case of elastoplasticity (see Okada et al. [9]). We briefly describe the formulations of present s-FEM.

We denote the displacement increments to be Δu_i^G and Δu_i^{Li} $(i=1,2,3,\cdots,n)$ that are based on the shape functions of finite elements of the global and the local models. The displacement functions are superposed when the global and the local mesh regions overlap each other. For example, for a region, where the global and the local mesh regions (Ω^{Lp}, Ω^{Lq} and Ω^{Lr}) overlap, we write the displacement increments Δu_i, as:

$$\Delta u_i = \Delta u_i^G + \Delta u_i^{Lp} + \Delta u_i^{Lq} + \Delta u_i^{Lr} \tag{50}$$

At a point, where any local models do not overlap with the global model, the displacements u_i equal u_i^G ($u_i = u_i^G$). The continuities of the displacements are enforced by letting the functions u_i^{L1}, u_i^{L2}, u_i^{L3}, $\cdots$, u_i^{Ln} be zero at the outer boundaries Γ^{Li} of the local model regions Ω^{Li}. The statement of principle of virtual work in an incremental formulation is written to be:

$$\int_{\Omega^G} \frac{\partial \Delta \delta u_i}{\partial x_j} D_{ijk\ell}^{Damage} \frac{\partial \Delta u_k}{\partial x_\ell} \mathrm{d}\Omega^G = \int_{\Gamma_t^G} \delta \Delta u_i \Delta \bar{t}_i \mathrm{d}\Gamma_t^G \tag{51}$$

where the variations of the displacements are defined in the same manner as the displacements. Γ_t^G denotes the boundary where the tractions $\bar{t}_i$ are prescribed. $D_{ijk\ell}^{Damage}$ are the forth order tensor representing material's stress-strain relationship (incremental constitutive law). We then substitute the displacements and their variations in the statement of principle of virtual work. After some algebraic manipulations, we have:

$$\int_{\Omega^G} \frac{\partial \Delta\delta u_i^G}{\partial x_j} D_{ijk\ell}^{Damage} \frac{\partial \Delta u_k^G}{\partial x_\ell} \mathrm{d}\Omega^G + \sum_{q=1}^{n} \int_{\Omega^{L1}} \frac{\partial \Delta\delta u_i^G}{\partial x_j} D_{ijk\ell}^{Damage} \frac{\partial \Delta u_k^{Lq}}{\partial x_\ell} \mathrm{d}\Omega^{Lq} = \int_{\Gamma_t^G} \delta u_i \Delta \bar{t}_i \mathrm{d}\Gamma_t^G \tag{52}$$

$$\begin{aligned} &\int_{\Omega^{Lp}} \frac{\partial \Delta\delta u_i^{Lp}}{\partial x_j} D_{ijk\ell}^{Damage} \frac{\partial \Delta u_k^G}{\partial x_\ell} \mathrm{d}\Omega^{Lp} + \int_{\Omega^{Lp}} \frac{\partial \Delta\delta u_i^{Lp}}{\partial x_j} D_{ijk\ell}^{Damage} \frac{\partial \Delta u_k^{Lp}}{\partial x_\ell} \mathrm{d}\Omega^{Lp} \\ &+ \sum_{\substack{q=1 \\ q\neq p}}^{n} \int_{\Omega^{Lp-Lq}} \frac{\partial \Delta\delta u_i^{Lq}}{\partial x_j} D_{ijk\ell}^{Damage} \frac{\partial \Delta u_k^{Lq}}{\partial x_\ell} \mathrm{d}\Omega^{Lp-Lq} = 0 \qquad (p = 1,2,3,\cdots,n) \end{aligned} \tag{53}$$

It is noted here that the right hand side of equation (53) equals zero, since the local model regions do not intersect with the outer boundary of the structure. Ω^{Lp-Lq} ($p,q = 1,2,3,\cdots,n;\ p \neq q$) denote regions sheared by Ω^{Lp} and Ω^{Lq} (i.e., $\Omega^{Lp-Lq} = \Omega^{Lp} \cap \Omega^{Lq}$). When $0 = \Omega^{Lp} \cap \Omega^{Lq}$, the related terms in equation (53) disappear. After the global and local regions are discretized by appropriate finite elements, we can write a matrix formulation, as:

$$\begin{Bmatrix} \Delta \boldsymbol{f}^G \\ \boldsymbol{0} \\ \boldsymbol{0} \\ \vdots \\ \boldsymbol{0} \end{Bmatrix} = \begin{bmatrix} \boldsymbol{K}^G & \boldsymbol{K}^{G-L1} & \boldsymbol{K}^{G-L2} & \cdots & \boldsymbol{K}^{G-Ln} \\ \boldsymbol{K}^{L1-G} & \boldsymbol{K}^{L1} & \boldsymbol{K}^{L1-L2} & \cdots & \boldsymbol{K}^{L1-Ln} \\ \boldsymbol{K}^{L2-G} & \boldsymbol{K}^{L2-L1} & \boldsymbol{K}^{L2} & \cdots & \boldsymbol{K}^{L2-Ln} \\ \vdots & \vdots & \vdots & \ddots & \vdots \\ \boldsymbol{K}^{Ln-G} & \boldsymbol{K}^{Ln-L1} & \boldsymbol{K}^{Ln-L2} & \cdots & \boldsymbol{K}^{Ln} \end{bmatrix} \begin{Bmatrix} \Delta \boldsymbol{u}^G \\ \Delta \boldsymbol{u}^{L1} \\ \Delta \boldsymbol{u}^{L2} \\ \vdots \\ \Delta \boldsymbol{u}^{Ln} \end{Bmatrix} \tag{54}$$

where $\Delta \boldsymbol{u}^G$ and $\Delta \boldsymbol{u}^{Lp}$ are the column vectors of unknown nodal displacements of the global and the local meshes. Matrices $\boldsymbol{K}^G$, $\boldsymbol{K}^{Lp}$, $\boldsymbol{K}^{G-Lp}$, $\boldsymbol{K}^{Lp-Lq}$ arise from the integrals in the left hand sides of equations (52) and (53). Since, $\boldsymbol{K}^{G-Lp} = \left(\boldsymbol{K}^{Lp-G}\right)^T$ and $\boldsymbol{K}^{Lp-Lq} = \left(\boldsymbol{K}^{Lq-Lp}\right)^T$, the global stiffness matrix in the right hand side of equation (54) is symmetric. However, the global stiffness matrix is not banded, unlike an ordinary finite element method. $\Delta \boldsymbol{f}^G$ is the consistent nodal force vector arising from the right hand side of equation (52).

The coefficient matrix of equation (54) is symmetric. However, the coefficient matrix looses its band structure, as there are many off-diagonal components. In such a case, use of iterative equation solver is advantageous over direct solvers. Thus, we adopted an Incomplete Cholesky-decomposition-preconditioned conjugate gradient (ICCG) method [10].

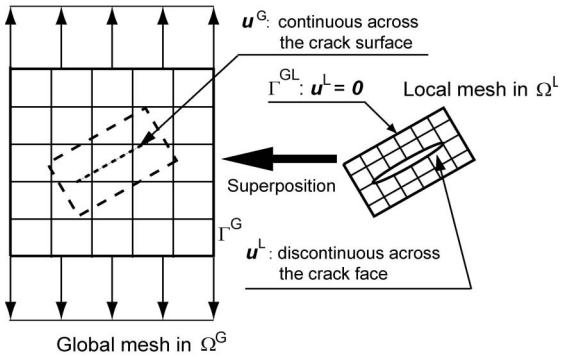

Figure 3 A schematic illustration for s-FEM (s-version finite element method) modeling. A crack problem is presented as an example.

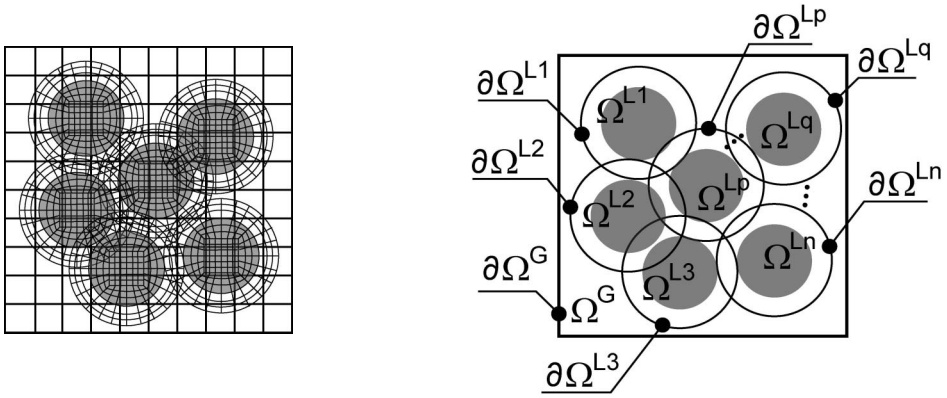

(a) s-FEM discretization (b) Global and local model regions

Figure 4 The s-FEM model with multiple local model regions that overlap each other.

2.2 Incremental algorithm

The constitutive equations were implemented in the s-FEM computer program. In present analysis, we did not implement equilibrium iteration scheme. The reason why we did not do so was that computations for nodal reaction forces became sometimes erroneous. Hence, equilibrium iteration algorithms such as Newton-Raphson scheme may not converge or may converge to wrong solutions. The displacements $u_i(x)$, stresses $\sigma_{ij}(x)$ and strains $\varepsilon_{ij}(x)$ at a point are expressed by the sum of their

increments $\Delta u_i^I(x)$, $\Delta\sigma_{ij}^I(x)$ and $\Delta\varepsilon_{ij}^I(x)$, as:

$$u_i(x) = \sum_I \Delta u_i^I(x), \quad \sigma_{ij}(x) = \sum_I \Delta\sigma_{ij}^I(x) \quad \text{and} \quad \varepsilon_{ij}(x) = \sum_I \Delta\varepsilon_{ij}^I(x) \tag{55}$$

All the other deformation parameters are treated in the same fashion.

2.3 Evaluation of relationship between the effective stress-like parameters and the damage parameters

The procedures that are described in sections 1.3 and 1.4 are implemented in the s-FEM computer program. Therefore, an analyst only needs to specify a one dimensional stress-strain relationship, Young's modulus and Poisson's ratio. The stress-strain relationship is given by specifying a series of data points on the curve [(σ_1,ε_1), (σ_2,ε_2), (σ_3,ε_3), $\bullet\bullet\bullet$, (σ_i,ε_i), $(\sigma_{i+1},\varepsilon_{i+1})$, $\bullet\bullet\bullet$]. The first data point (σ_1,ε_1) must be on the line of elastic slope, i.e.; $\sigma_1 = E\varepsilon_1$, where E is the Young's modulus.

Thus, the analyst does not have to deal with the tedious procedures of sections 1.3 and 1.4 and the input data structure is very analogous to that of isotropic elastoplasticity.

2.4 Some other issues associated with the damage constitutive law-initiation of nonlinear deformation

Material initially undergoes elastic deformation and then follows nonlinear deformation path. That is analogous to the case of elastoplasticity. In this section, algorithms when the nonlinear deformation initiates at a point during an increment are discussed. First, we deal with the case of isotropic damage.

Let us assume that uniaxial stress-strain curve is given as shown in Figure 5. The stress-strain relationship upto (σ_1,ε_1) is linear (no damage) and the nonlinear deformation initiates at (σ_1,ε_1). Then, by following the procedures in section 1.3, the sets of effective stress and damage parameter corresponding to (σ_2,ε_2), (σ_3,ε_3), $\bullet\bullet\bullet$, (σ_i,ε_i), $(\sigma_{i+1},\varepsilon_{i+1})$, $\bullet\bullet\bullet$ are determined to be $(\bar{\tau}_1,d_1)$, $(\bar{\tau}_2,d_2)$, $(\bar{\tau}_3,d_3)$, $\bullet\bullet\bullet$, $(\bar{\tau}_i,d_i)$, $(\bar{\tau}_{i+1},d_{i+1})$, $\bullet\bullet\bullet$. We assume that the state of stresses σ_{ij}^I and strains ε_{ij}^I at the

beginning of I th incremental step satisfies:

$$C_{ijk\ell}\varepsilon_{ij}^{I}\varepsilon_{k\ell}^{I} < \bar{\tau}_1^2 \tag{56}$$

It is also assumed that during the I th incremental step, material damage starts taking place. Therefore, we can write:

$$C_{ijk\ell}\left(\varepsilon_{ij}^{I}+\Delta\varepsilon_{ij}^{I}\right)\left(\varepsilon_{k\ell}^{I}+\Delta\varepsilon_{k\ell}^{I}\right) > \bar{\tau}_1^2 \tag{57}$$

Thus, the I th incremental step can be split into elastic and nonlinear part. We let the their fractions to be α and $1-\alpha$. Hence, the following equation holds:

$$C_{ijk\ell}\left(\varepsilon_{ij}^{I}+\alpha\Delta\varepsilon_{ij}^{I}\right)\left(\varepsilon_{k\ell}^{I}+\alpha\Delta\varepsilon_{k\ell}^{I}\right) = \bar{\tau}_1^2 \tag{58}$$

From equation (58), we can determine the value of α.

$$\begin{aligned} 0 &= C_{ijk\ell}\left(\varepsilon_{ij}+\alpha\Delta\varepsilon_{ij}\right)\left(\varepsilon_{k\ell}+\alpha\Delta\varepsilon_{k\ell}\right)-\bar{\tau}_1^2 \\ &= \left(C_{ijk\ell}\varepsilon_{ij}\varepsilon_{k\ell}-\bar{\tau}_1^2\right)+2\alpha C_{ijk\ell}\varepsilon_{ij}\Delta\varepsilon_{k\ell}+\alpha^2 C_{ijk\ell}\Delta\varepsilon_{ij}\Delta\varepsilon_{k\ell} \\ &= C+2\alpha B+\alpha^2 A \end{aligned} \tag{59}$$

where $C<0$ and $A>0$, since the damage state has not yet been reached and the quadratic form of $C_{ijk\ell}$ is positive definite. α can be determined to be:

$$\alpha = \frac{-2B\pm\sqrt{4B^2-4AC}}{2A} = \frac{-B\pm\sqrt{B^2-AC}}{A} \tag{60}$$

Since $C<0$ and $A>0$, $AC<0$. We take the positive sign, in order for α to be a positive number. Therefore, we have:

$$\alpha = \frac{-B+\sqrt{B^2-AC}}{A} \tag{61}$$

Thus, the increments $\Delta\sigma_{ij}^{I}$ of stresses during the I th incremental step can be written to be:

$$\Delta\sigma_{ij}^{I} = C_{ijk\ell}\left(\alpha\Delta\varepsilon_{ij}^{I}\right) + \left(1-\alpha\right)\left\{C_{ijk\ell}\Delta\varepsilon_{k\ell}^{I} - \frac{H^{1}}{\bar{\tau}^{1}}\left(\sigma_{ij}^{I} + \alpha C_{ijmn}\Delta\varepsilon_{mn}^{I}\right)\left(\sigma_{k\ell}^{I} + \alpha C_{k\ell pq}\Delta\varepsilon_{pq}^{I}\right)\Delta\varepsilon_{k\ell}^{I}\right\} \quad (62)$$

For the separate Isotropic/deviatoric damage model, the similar procedures can be established. They are described below.

First, we assume that a uniaxial stress-strain curve as depicted in Figure 5 is given. We extract a series of data on effective stresses and damage parameters $\left(d_V\big|_1, d_D\big|_1, \bar{\tau}_V\big|_1, \bar{\tau}_D\big|_1\right)$, $\left(d_V\big|_2, d_D\big|_2, \bar{\tau}_V\big|_2, \bar{\tau}_D\big|_2\right)$, $\left(d_V\big|_3, d_D\big|_3, \bar{\tau}_V\big|_3, \bar{\tau}_D\big|_3\right)$, $\bullet\bullet\bullet$, $\left(d_V\big|_i, d_D\big|_i, \bar{\tau}_V\big|_i, \bar{\tau}_D\big|_i\right)$, $\left(d_V\big|_{i+1}, d_D\big|_{i+1}, \bar{\tau}_V\big|_{i+1}, \bar{\tau}_D\big|_{i+1}\right)$, $\bullet\bullet\bullet$ from the stress and strain data $(\sigma_1, \varepsilon_1)$, $(\sigma_2, \varepsilon_2)$, $(\sigma_3, \varepsilon_3)$, $\bullet\bullet\bullet$, $(\sigma_i, \varepsilon_i)$, $(\sigma_{i+1}, \varepsilon_{i+1})$, $\bullet\bullet\bullet$. We assume that the states of stresses and strains (σ_{ij}^{I}, ε_{ij}^{I}) and (σ_{ij}^{J}, ε_{ij}^{J}) at the beginning of I th and J th incremental step satisfy:

$$2\mu\varepsilon_{ij}^{\prime I}\varepsilon_{ij}^{\prime I} < \left(\bar{\tau}_V\big|_1\right)^2 \quad (63)$$

$$K\left(\varepsilon_{kk}^{J}\right)^2 < \left(\bar{\tau}_D\big|_1\right)^2 \quad (64)$$

Then, it is also assumed that, during the I th and J th incremental step, deviatoric and dilatational damage start taking place. Thus, we can write:

$$2\mu\left(\varepsilon_{ij}^{\prime I} + \Delta\varepsilon_{ij}^{\prime I}\right)\left(\varepsilon_{ij}^{\prime I} + \Delta\varepsilon_{ij}^{\prime I}\right) > \left(\bar{\tau}_V\big|_1\right)^2 \quad (65)$$

$$K\left(\varepsilon_{kk}^{J} + \Delta\varepsilon_{kk}^{J}\right)^2 > \left(\bar{\tau}_D\big|_1\right)^2 \quad (66)$$

The I th and J th increments are split into two portions that are elastic and nonlinear parts. The fractions of the elastic parts are specified to be α^I and α^J. Thus, we can write:

$$2\mu\left(\varepsilon'^I_{ij} + \alpha^I \Delta\varepsilon'^I_{ij}\right)\left(\varepsilon'^I_{ij} + \alpha^I \Delta\varepsilon'^I_{ij}\right) = \left(\bar{\tau}_D\big|_1\right)^2 \tag{67}$$

$$K\left(\varepsilon^J_{kk} + \alpha^J \Delta\varepsilon^J_{kk}\right)^2 = \left(\bar{\tau}_V\big|_1\right)^2 \tag{68}$$

Then, α^I and α^J can be determined. From equation (67), we obtain:

$$\left(\alpha^I\right)^2 \Delta\varepsilon'^I_{ij}\Delta\varepsilon'^I_{ij} + 2\alpha^I \varepsilon'^I_{ij}\Delta\varepsilon'^I_{ij} + \varepsilon'^I_{ij}\varepsilon'^I_{ij} - \frac{\left(\bar{\tau}_D\big|_1\right)^2}{2\mu} = 0 \tag{69}$$

By letting $A^D = \Delta\varepsilon'^I_{ij}\Delta\varepsilon'^I_{ij}$, $B^D = \varepsilon'^I_{ij}\Delta\varepsilon'^I_{ij}$ and $C = \varepsilon'^I_{ij}\varepsilon'^I_{ij} - \frac{\left(\bar{\tau}_D\big|_1\right)^2}{2\mu}$, we arrive at:

$$\alpha^I = \frac{-2B^D \pm \sqrt{4\left(B^D\right)^2 - 4A^D C^D}}{2A^D} = \frac{-B^D \pm \sqrt{\left(B^D\right)^2 - A^D C^D}}{A^D} \tag{70}$$

In equation (70), it is appropriate to choose the positive sign. Therefore, we have:

$$\alpha^I = \frac{-B^D + \sqrt{\left(B^D\right)^2 - A^D C^D}}{A^D} \tag{71}$$

From equation (68), we obtain:

$$\left(\alpha^J\right)^2\left(\Delta\varepsilon^J_{kk}\right)^2 + 2\alpha^J \varepsilon^J_{kk}\Delta\varepsilon^J_{kk} + \left(\varepsilon^J_{kk}\right)^2 - \frac{\left(\bar{\tau}_V\big|_1\right)^2}{K} = 0 \tag{72}$$

Thus, equation (72) is solved for α^J by letting $A^V = \left(\Delta\varepsilon^J_{kk}\right)^2$, $B^V = \varepsilon^J_{kk}\Delta\varepsilon^J_{\ell\ell}$ and $C^V = \left(\varepsilon^J_{kk}\right)^2 - \frac{\left(\bar{\tau}_V\big|_1\right)^2}{K}$ and we have:

$$\alpha^{J} = \frac{-B^{V} + \sqrt{\left(B^{V}\right)^{2} - A^{V}C^{V}}}{A^{V}} \tag{73}$$

In equation (73), the appropriate sign associated with $\sqrt{\left(B^{V}\right)^{2} - A^{V}C^{V}}$ has already been chosen. The increments of the deviatoric and hydrostatic stresses during the I th and the J th incremental steps are written to be:

$$\Delta\sigma_{ij}^{\prime I} = 2\left(1-d_{D}\right)\mu\Delta\varepsilon_{ij}^{\prime I} - \left(1-\alpha\right)\frac{4H_{D}\left(\bar{\tau}_{D}, d_{D}\right)}{\bar{\tau}_{D}}\mu^{2}\varepsilon_{ij}^{\prime I}\varepsilon_{k\ell}^{\prime I}\Delta\varepsilon_{k\ell}^{\prime I} \tag{74}$$

$$\frac{1}{3}\Delta\sigma_{kk}^{J} = \left(1-d_{V}\right)K\Delta\varepsilon_{kk}^{J} - \left(1-\alpha\right)\frac{H_{V}\left(\bar{\tau}_{V}, d_{V}\right)}{\bar{\tau}_{V}}\left(K\varepsilon_{kk}^{J}\right)^{2}\Delta\varepsilon_{\ell\ell}^{J} \tag{75}$$

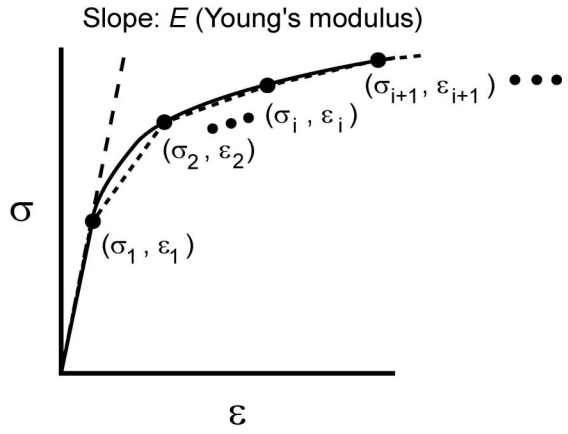

Figure 5 An illustration of stress-strain curve and its transition from the linear (elastic) to nonlinear (damage) deformation.

3. Numerical demonstrations of s-FEM computer program with the damage constitutive laws

In this chapter, the s-FEM program that is developed during this course of study is demonstrated. Example problems that contain one or two particles in a unit cell region are solved.

3.1 Stress-strain relationship

Stress-strain curve was taken from Kwon and Liu [11] and is shown in Figure 6. We then extract a series of data points (σ_1,ε_1), (σ_2,ε_2), (σ_3,ε_3),•••, (σ_7,ε_7), as also shown in Figure 6. As an example, the relationship between the uniaxial strain and the damage parameter for the case of isotropic damage is depicted in Figure 7. Thus, the uniaxial stress-strain curve is reconstructed by a series of linear approximations, as shown in Figure 8.

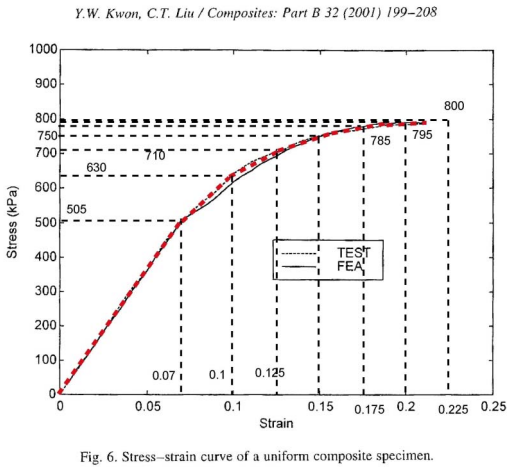

Fig. 6. Stress–strain curve of a uniform composite specimen.

Figure 6 Uniaxial stress-strain curve of polymeric particulate composite material that was given in Kwon and Liu [11]

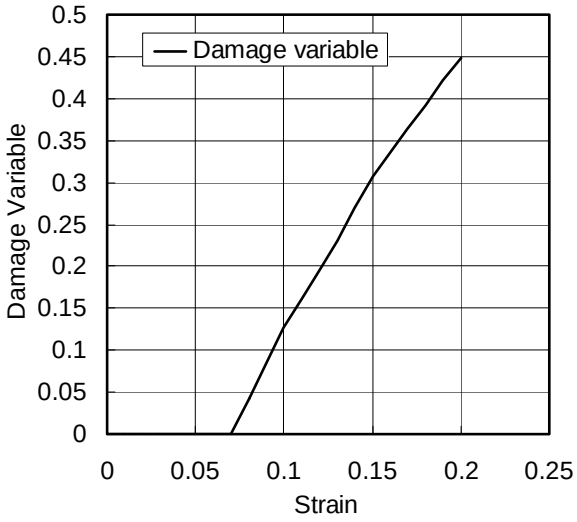

Figure 7 Relationship between the strain and the damage parameter for the isotropic damage constitutive model, which was extracted from the stress-strain curve of Figure 6.

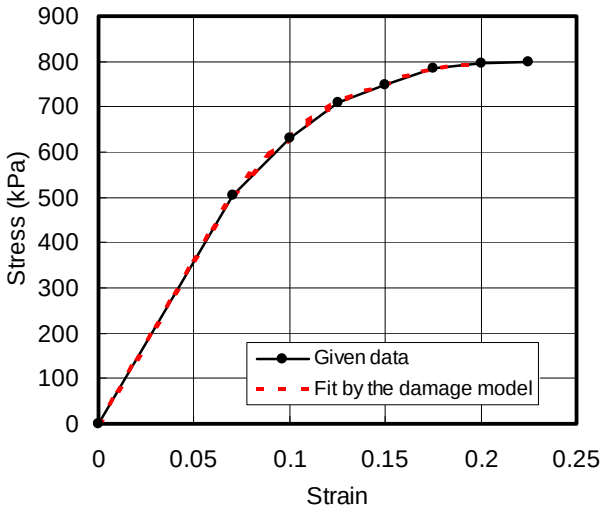

Figure 8 Uniaxial stress-strain curve that was reconstructed after the relationship between the effective stress-like and the damage parameters is established by the proposed procedures.

3.2 Example problem-isotropic damage model

In this section a simple example problem that demonstrates the isotropic damage constitutive model is presented. A block containing two hard particles subject to tension, as depicted in Figure 9, is solved. To model it, we used the s-FEM approach. The particle and its vicinity were discretized by local model and the block as whole was modeled by the global one. They are shown in Figure 10.

In Figure 11~14, the distributions of stress and the evolution of damage parameter at a section cutting through the center of the particle are shown. It is seen that the material damage develops at the top and bottom of the particles. The damage region connects the particles.

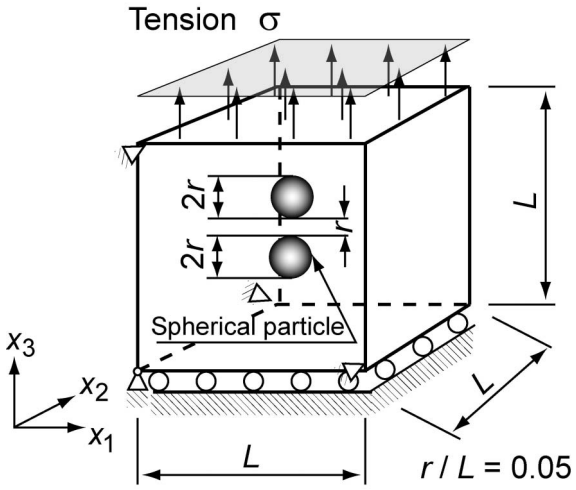

Figure 9 A cubical block containing two particles, subject to tensioin.

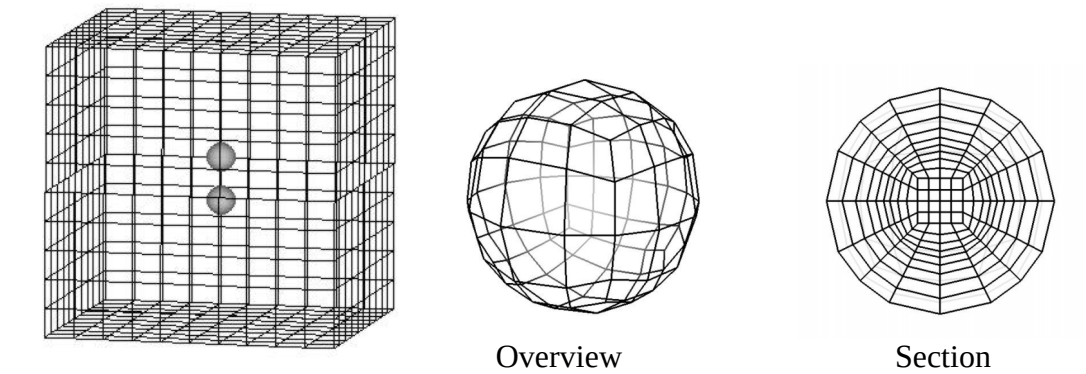

(a) Global finite element model (b) Local finite element model

Figure 10 The global and local finite element models for the s-FEM analysis.

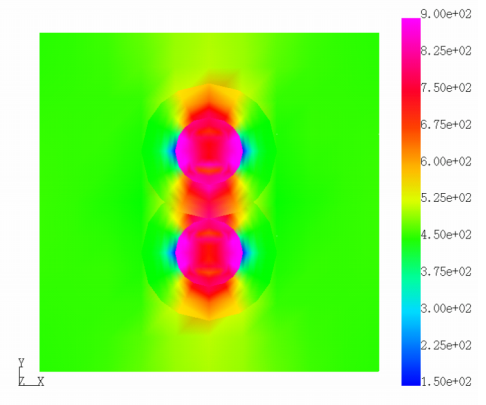

Figure 11 Tensile stress distribution at the tensile strain 6.32×10^{-2}

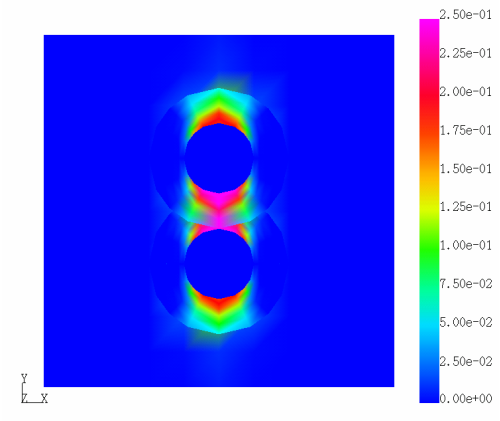

Figure 12 Distribution of the damage parameter at the tensile strain 6.32×10^{-2}

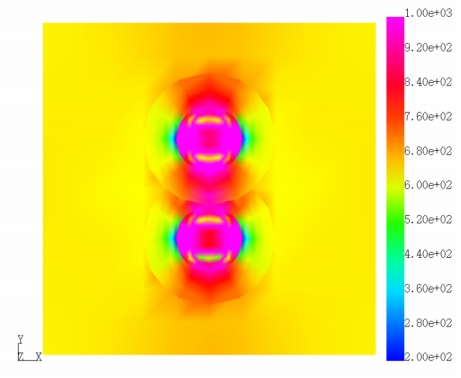

Figure 13 Tensile stress distribution at the tensile strain 10.0×10^{-2}

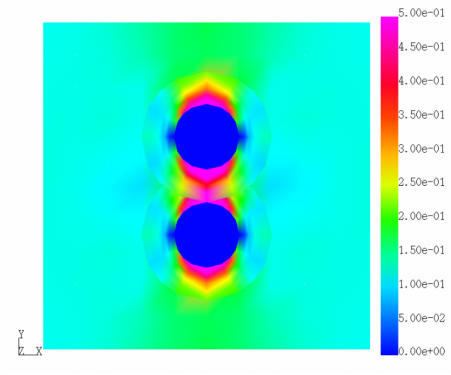

Figure 14 Distribution of the damage parameter at the tensile strain 10.0×10^{-2}

3.3 Example problem-separate Isotropic/deviatoric damage model

The separate isotropic/deviatoric damage model is also tested for the same problem. The constants α which determines the ratio of contributions of hydrostatic pressure and deviatoric stress was varied (0.1, 1.0, 10.0). When $\alpha = 0.1$, the contribution of the hydrostatic pressure dominates that of the deviatoric stresses. When $\alpha = 1.0$, the material response should be very similar to that of the isotropic damage case. When $\alpha = 10.0$, the deviatoric stress components should have the major contribution.

In Figures 15, 16 and 17, the distributions of stress and the damage parameters in a section that cuts through the center of the particles are depicted for $\alpha = 0.1$, $\alpha = 0.99$

and $\alpha = 10.0$, respectively. The reason why we did not let α be 1.0 was that $\alpha = 1.0$ requires a special program implementation in the procedures which are described in section 1.4.

In the case of $\alpha = 0.1$, it is seen that the magnitude of dilatational damage parameter is much larger than that of the deviatoric one. Therefore, as we intended, the dilatational damage is the major damage mode. When $\alpha = 0.99$, the magnitudes of the dilatational and deviatoric damage parameters are similar. For $\alpha = 10.0$, the value of the deviatoric damage parameter is much larger than that of the dilatational one. In this case also, the material behaves as we intended.

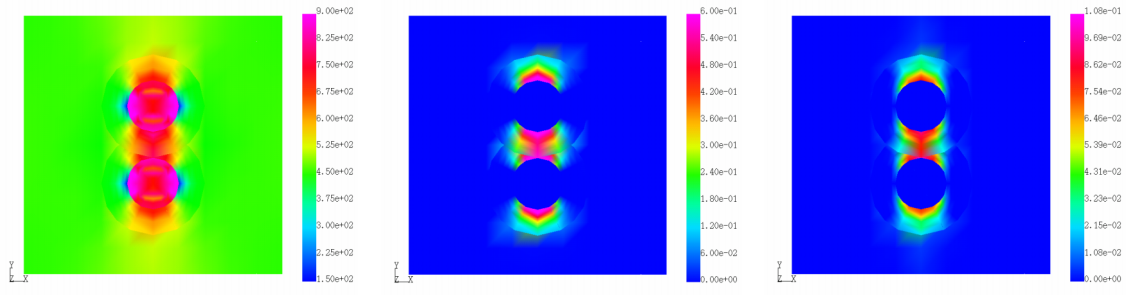

Tensile stress | Volumetric damage parameter | Deviatoric damage parameter

(a) Tensile strain 6.32×10^{-2}

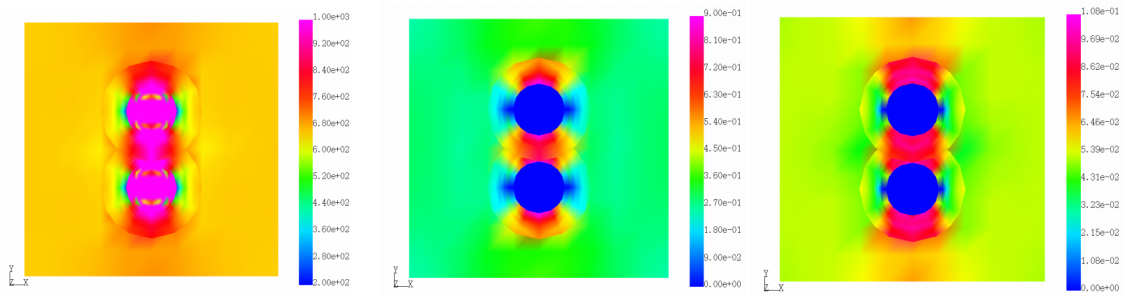

Tensile stress | Volumetric damage parameter | Deviatoric damage parameter

(b) Tensile strain 10.0×10^{-2}

Figure 15 The distributions of tensile stress and the damage parameters in the section cutting through two particles when the separate dilatational/deviatoric damage constitutive model with $\alpha = 0.1$ is used.

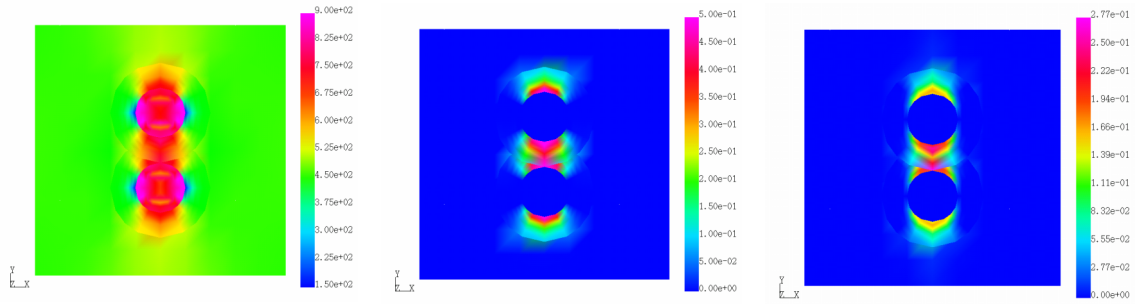

Tensile stress | Volumetric damage parameter | Deviatoric damage parameter

(a) Tensile strain 6.32×10^{-2}

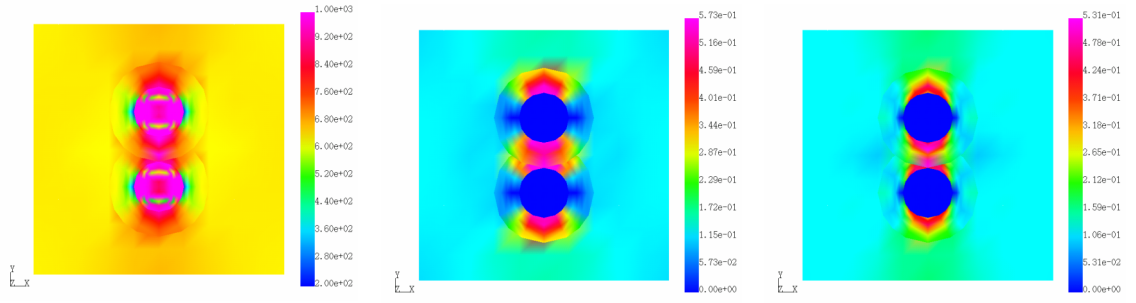

Tensile stress | Volumetric damage parameter | Deviatoric damage parameter

(b) Tensile strain 10.0×10^{-2}

Figure 16 The distributions of tensile stress and the damage parameters in the section cutting through two particles when the separate dilatational/deviatoric damage constitutive model with $\alpha = 0.99$ is used.

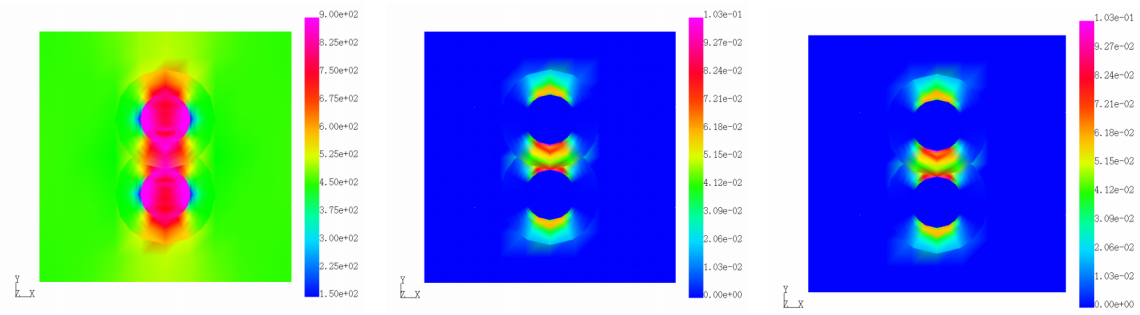

Tensile stress | Volumetric damage parameter | Deviatoric damage parameter

(a) Tensile strain 6.32×10^{-2}

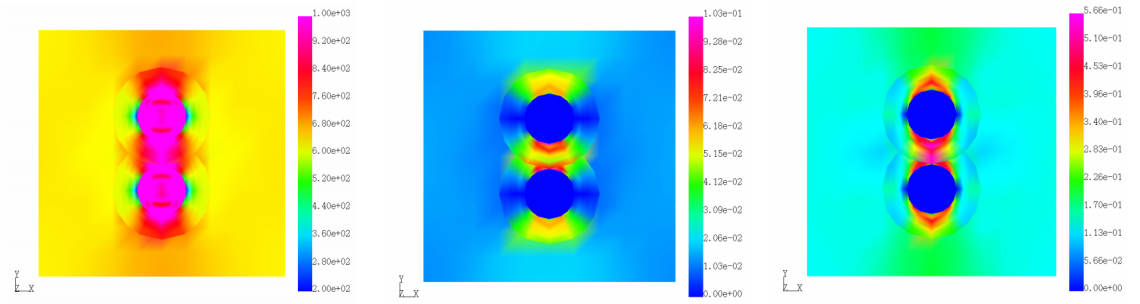

Tensile stress | Volumetric damage parameter | Deviatoric damage parameter

(b) Tensile strain 10.0×10^{-2}

Figure 17 The distributions of tensile stress and the damage parameters in the section cutting through two particles when the separate dilatational/deviatoric damage constitutive model with $\alpha = 10.0$ is used.

3.4 Summary-Numerical demonstrations on the damage constitutive models and the s-FEM computer program

The damage constitutive models are tested in this chapter. We found that material damages accumulate at the locations of the stress concentration. The damage regions connect between the particles.

The separate isotropic/deviatoric damage model could control the damage mode. The intended damage mode (dilatational or deviatoric) dominates the other.

4. Investigating the Effects of Micro-Structure on the Tensile Behavior of a Solid Propellant

Having developed the damage models and the s-FEM computer program, we carried out a series of analyses on the tensile behavior of a block made of polymeric particulate composite material. Thought the particles distribute evenly in a macroscopic sense, they have some distributions at a microscopic level. In order to investigate the effects of the locally uneven distributions of the particles, we assume that the variations in material stiffness at a local level. Experimental evidences showed that when representative volume of larger than 2.0 mm by 2.0 mm the material could be treated as a homogeneous material. This means that if one took the representative volume equal to or larger than 2.0 mm by 2.0 mm the volume fraction of particles is approximately the same throughout the block.

The reference stress-strain curve was taken from Kwon and Liu [11]. Magnification factors are multiplied and six different stress-strain curves (level -2.5, -1.5, -0.5, 0.5, 1.5, 2.5) were generated as shown in Figure 18. Then, by using a random number generator with Gaussian distribution, a series of random numbers are generated and are assigned to finite elements. Material data is assigned to each finite element according to the value of assigned random number. For example, when the value of assigned random number is between $-\rho$ and $-\rho/2$, the stress-strain curve of level -1.5 is assigned to the element. The relationships between the assigned random number and the level of stress-strain curve to be used are shown in Figure 19 and Table 1.

Table 1 The relationship between the assigned random number and the level of stress-strain curve to be adopted.

Random number V	$V < -\rho$	$-\rho \le V < -0.5\rho$	$-0.5\rho \le V < 0$	$0 \le V < 0.5\rho$	$0.5\rho \le V < \rho$	$\rho \le V$
Level	-2.5	-1.5	-0.5	0.5	1.5	2.5
Magnification Factor	0.75	0.85	0.95	1.05	1.15	1.25

Two different analysis models were generated by specifying different initial values to the random number generator. They are different but are statistically the same. The models are shown in Figure 20. The finite element model is shown in Figure 21. There are 20000 finite elements. The size of finite element is less than 0.2 mm. Therefore,

there are at least 100 elements inside the 2.0 mm by 2.0 mm representative area.

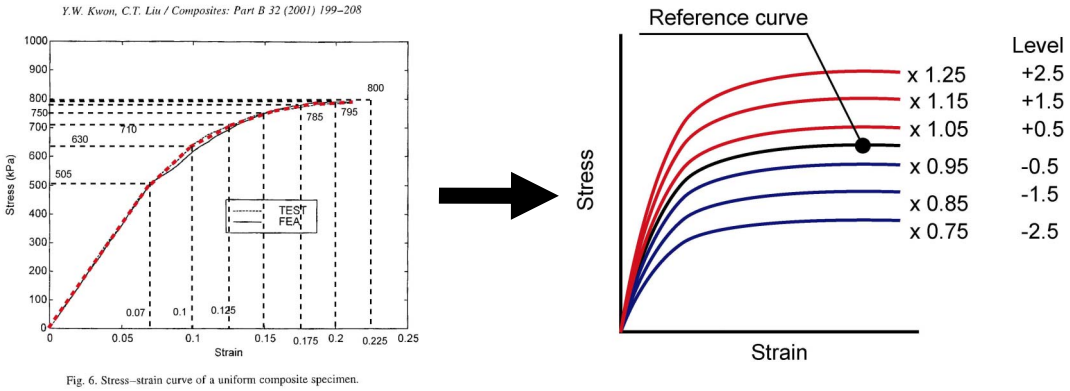

Figure 18 Six level stress-strain relationships that were postulated in present investigation.

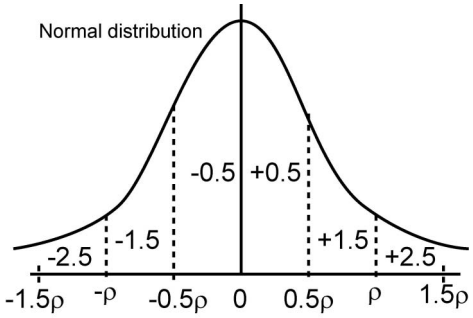

Figure 19 Relationship between the levels of the postulated stress-strain curves and the value of generated random number.

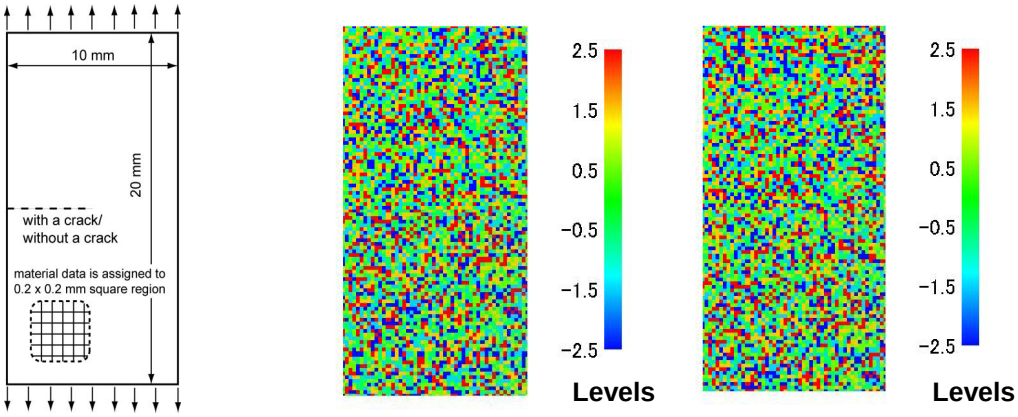

(a) Model #1 (b) Model #2

Figure 20 Two different analysis models that have the statically the same distributions of material stiffness.

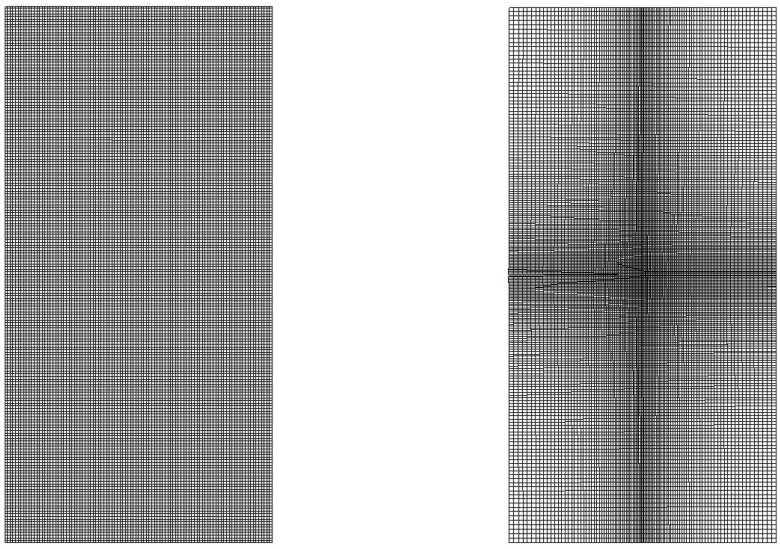

(a) Tension block (b) With a crack

Figure 21 The finite element analysis models

4.1 The behavior of a tensile block-Isotropic damage constitutive model

In this section, the tensile behavior of a block that was made of the isotropic continuum damage solid is presented. Stress-strain curve at a material point was set by the procedures that are presented in the previous section. The block was subject to 15% of tensile strain.

In Figure 22, the distributions of stress in the tensile direction when the block is subject to 0.3% of the strain are depicted. In this step, all the material points in the blocks have not undergone any material damage. Stress distributions show that the regions of low and high stresses run in the direction of loading.

In Figure 23, the distributions of the stress when the block is subject to 10% of tensile strain are shown. The trends in the figures are the same as those in Figure 22. In Figure 24, the distributions of the isotropic damage parameter are presented. Figure 24 shows that major trends in two different statistically the same blocks are the same. The regions of relatively sever damage run in about 45 degree from the axis of loading. However, it is seen that the regions of very sever damage run perpendicular to the tensile axis.

In Figure 25, the distributions of the stress when the block is subject to 15% of strain are depicted. The major trends are the same as Figures 21 and 23. The regions of high and low stresses run vertically. The distributions of the damage parameter are shown in Figure 26. The major trends are the same between two cases that are statistically the same. It is seen that many regions of sever damage run in short distances, typically equal or shorter than 1 mm, perpendicular to the direction of loading. Then, they link each other making larger damaged regions. The larger damaged regions run in various directions.

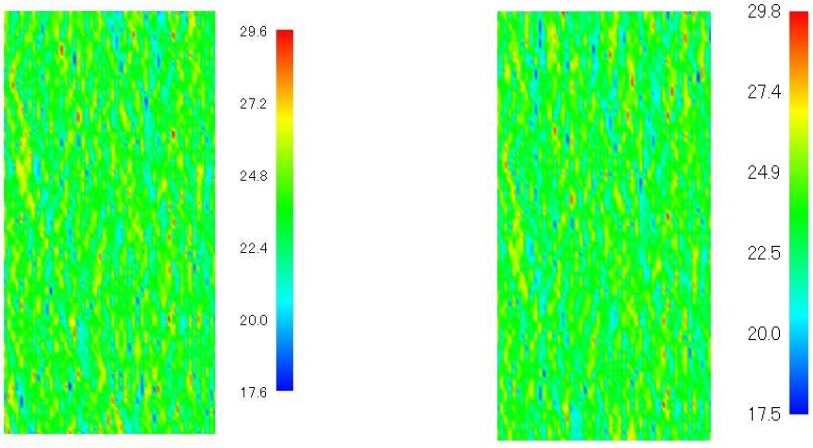

(a) Model #1 (b) Model #2

Figure 22 Tensile stress distributions when the blocks are subject to 0.3% of strain (elastic stage).

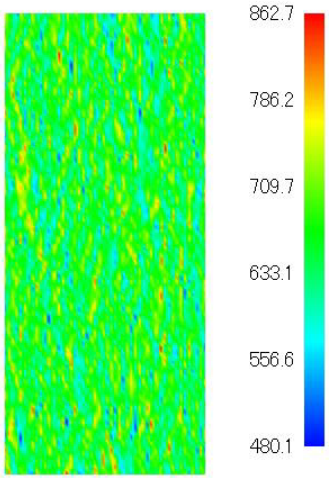

(a) Model #1

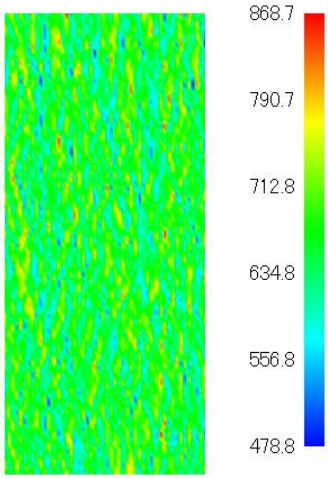

(b) Model #2

Figure 23 Tensile stress distributions when the blocks are subject to 10% of strain.

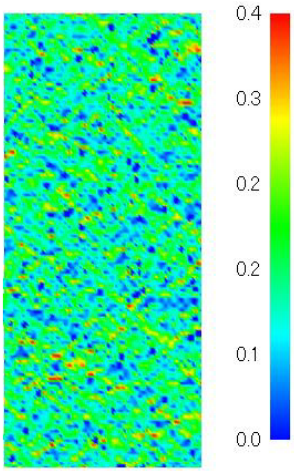

(a) Model #1

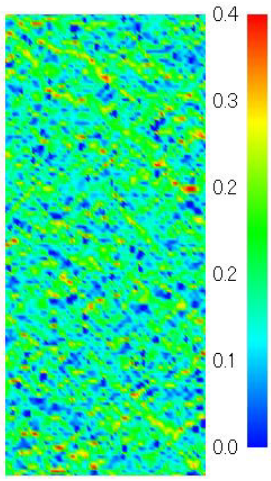

(b) Model #2

Figure 24 The distributions of the damage parameter when the blocks are subject to 10% of strain.

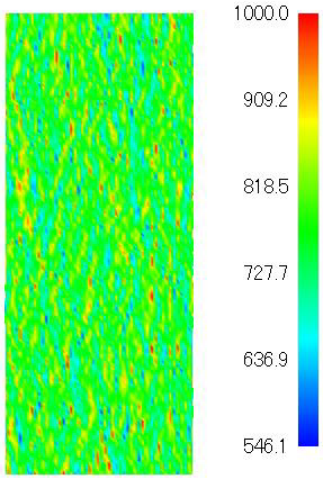

(a) Model #1

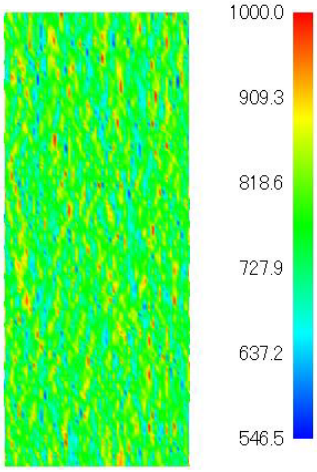

(b) Model #2

Figure 25 Tensile stress distributions when the blocks are subject to 15% of strain.

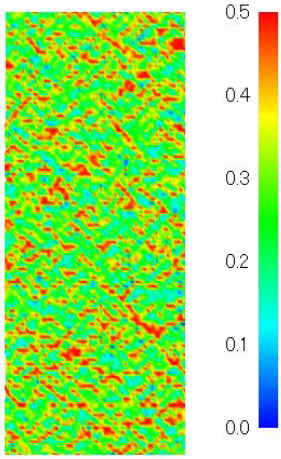

(a) Model #1

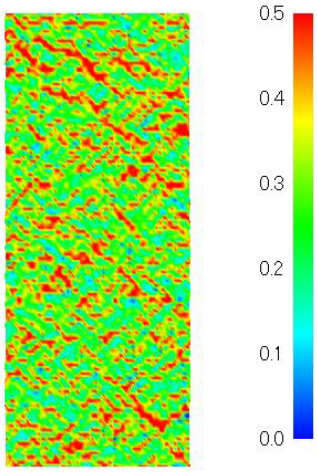

(b) Model #2

Figure 26 The distributions of the damage parameter when the blocks are subject to 15% of strain.

4.2 The behavior of a tensile block- separate Isotropic/deviatoric damage model

In this section, the tensile behavior of the block that was analyzed by the separate isotropic/deviatoric damage model is presented. The parameter α which characterizes the ratio of contribution of the volumetric and deviatoric damage modes was set to be 0.1, 0.99 or 10.0. These values correspond to the cases (1) the volumetric damage

dominates the deviatoric one, (2) both damage modes have the same levels of contributions and (3) the deviatoric damage mode dominates the volumetric one. They are compared with each other.

In Figures 27 (a) and (b), the effective stress-strain curves when model #1 and #2 are used are presented, respectively. It is seen that the macroscopic behavior of both the models are almost the same. In Figures 28-33, the distributions of stress and the damage parameters for model #1 are depicted. The stress distributions at 10% of strain are shown in Figure 28 (a)-(d). The distributions look alike. However, the distributions of the volumetric damage parameters are quite different from each other, as shown in Figures 29 (a)-(d). The value of damage parameter for $\alpha = 10.0$ is very small. For the cases of $\alpha = 0.1$ and $\alpha = 0.99$, regions with relatively large volumetric damage parameter d_V run perpendicular to the loading axis. In Figures 30 (a)-(d), the distributions of the deviatoric damage parameter d_D, when the block is subject to 10% of tensile strain, are depicted. The damage parameter throughout the block is very small as shown in Figure 30 (b) for the choice of parameter $\alpha = 0.1$. The locations/shapes of relatively low and high damages are the same for all the cases. However, it is clear that, for $\alpha = 10.0$, the regions of large damage parameter run in 45 degree direction form the loading axis. The trends are similar to the case of isotropic damage. However, the separate volumetric/deviatoric damage model with $\alpha = 10.0$ gives more pronounced result.

Figures 31 (a)-(d) show the distributions of tensile stress when the block is subject to 15% of strain. For all the cases in Figure 31 (a)-(d), the regions of high and low stresses run in the vertical direction. The concentrations of the stress are more pronounced in the case of $\alpha = 10.0$ than the other cases. The distributions in Figures 31 (a), (b) and (c) look very similar. In Figures 32 (a)-(d), the distributions of the volumetric damage parameter are depicted. Volumetric damage regions run in the horizontal direction when $\alpha = 0.1$ is assumed. For the cases of $\alpha = 0.99$ and $\alpha = 10.0$, the distributions look more uniform than that of $\alpha = 0.1$. There are localized areas with relatively small value of the damage parameter. When $\alpha = 10.0$ is adopted, the value of the damage parameter is small throughout the block. In Figures 33 (a)-(d), the distributions of deviatoric damage parameter are depicted. As expected, the value is small throughout the block when $\alpha = 0.1$. In the cases of $\alpha = 0.99$ and $\alpha = 10.0$, the distributions are similar to each other. There are the bands of large value of the damage parameter that run along 45 degree direction from the loading axis. The directions of the bands are slightly different from

the case of the isotropic damage model.

From the results presented in this section, it is clear that the bands of large volumetric damage parameter run in perpendicular to the loading direction, whereas those of large deviatoric damage parameter are along the 45 degree direction from the tensile axis. The results also show that the constant α can control which damage mode, volumetric or deviatoric, dominates the other. In Figures 34-39, the results obtained based on the model #2 are shown. The overall trends are the same as those obtained based on the model #1.

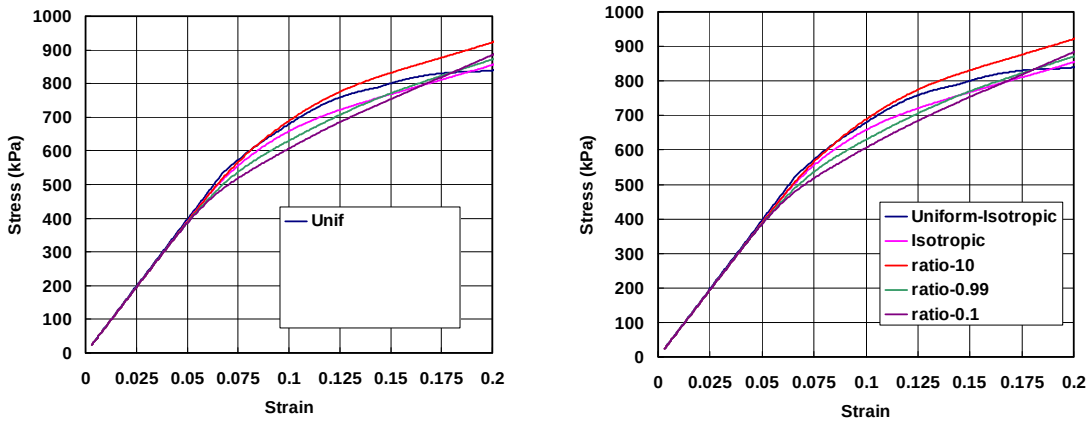

(a) Model #1 (b) Model #2

Figure 27 Effective stress-strain behaviors that were generated by the damage constitutive models with the material stiffness distribution models #1 and #2.

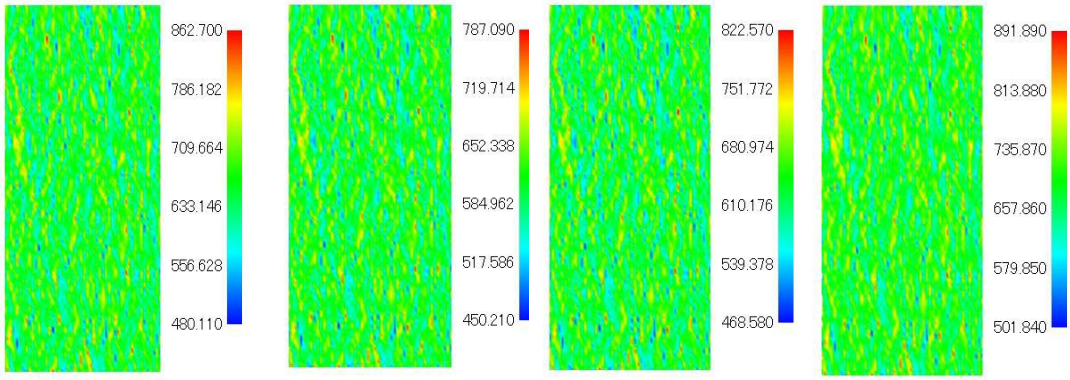

(a) Isotropic damage model (b) $\alpha = 0.1$ (c) $\alpha = 0.99$ (d) $\alpha = 10.0$

Figure 28 Tensile stress distributions at 10% overall tensile strain [(a) isotropic damage model, (b) separate dilatational/deviatoric damage model with $\alpha = 0.1$, (c) with $\alpha = 0.99$ and (d) with $\alpha = 10.0$].

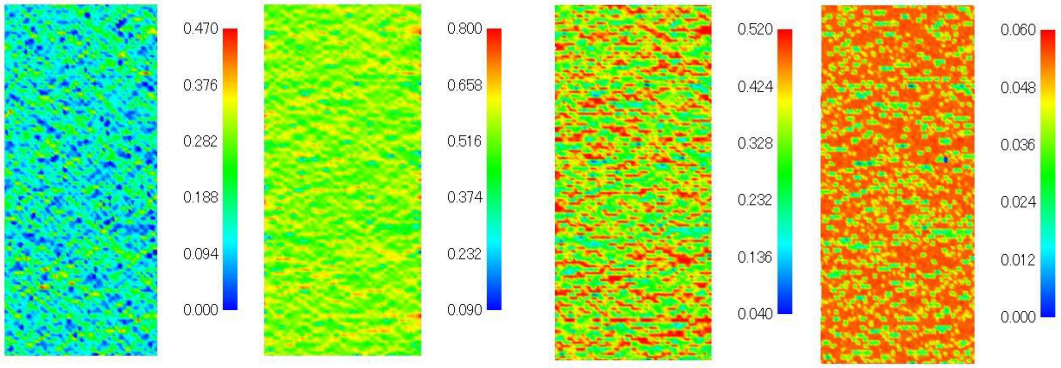

(a) Isotropic damage model (b) $\alpha = 0.1$ (c) $\alpha = 0.99$ (d) $\alpha = 10.0$

Figure 29 The distributions of dilatational damage parameter at 10% overall tensile strain [(a) isotropic damage model (the isotropic damage parameter), (b) separate dilatational/deviatoric damage model with $\alpha = 0.1$, (c) with $\alpha = 0.99$ and (d) with $\alpha = 10.0$].

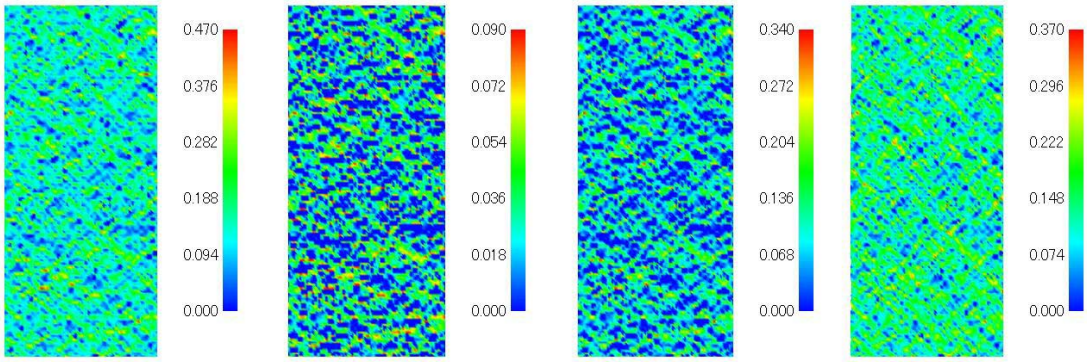

(a) Isotropic damage model (b) $\alpha = 0.1$ (c) $\alpha = 0.99$ (d) $\alpha = 10.0$

Figure 30 The distributions of deviatoric damage parameter at 10% overall tensile strain [(a) isotropic damage model (the isotropic damage parameter), (b) separate dilatational/deviatoric damage model with $\alpha = 0.1$, (c) with $\alpha = 0.99$ and (d) with $\alpha = 10.0$].

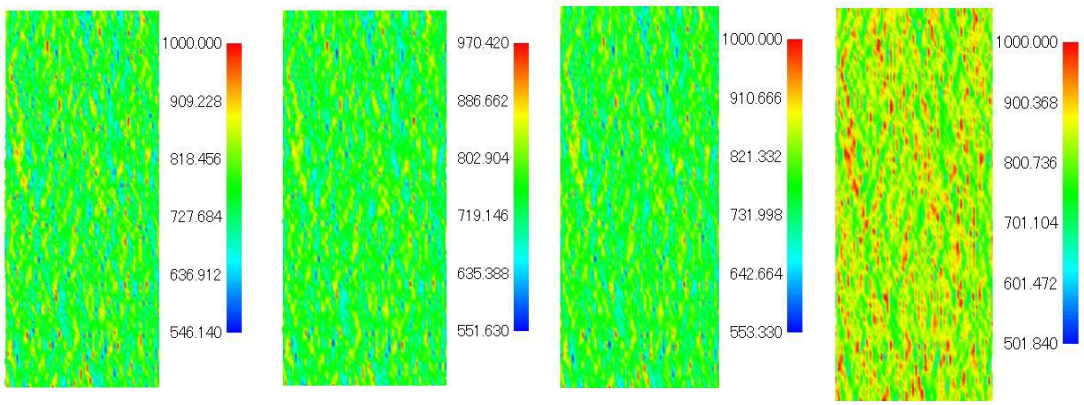

(a) Isotropic damage model (b) $\alpha = 0.1$ (c) $\alpha = 0.99$ (d) $\alpha = 10.0$

Figure 31 Tensile stress distributions at 15% overall tensile strain [(a) isotropic damage model, (b) separate dilatational/deviatoric damage model with $\alpha = 0.1$, (c) with $\alpha = 0.99$ and (d) with $\alpha = 10.0$].

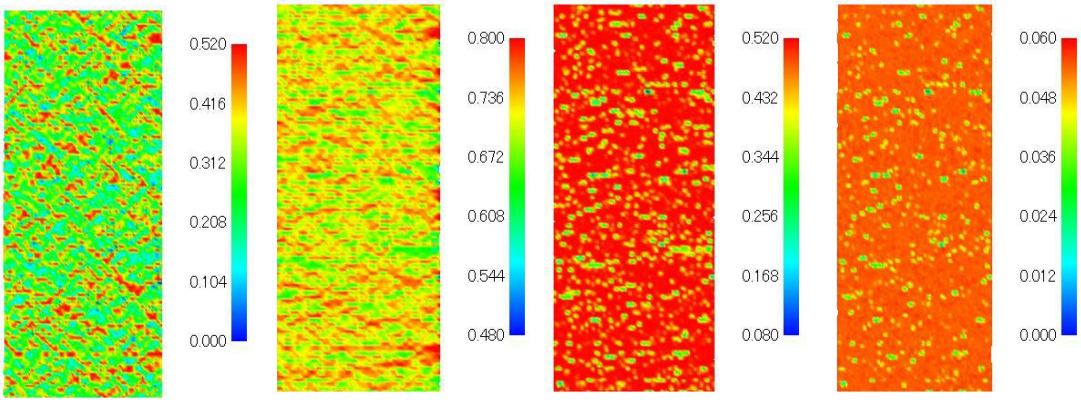

(a) Isotropic damage model (b) $\alpha = 0.1$ (c) $\alpha = 0.99$ (d) $\alpha = 10.0$

Figure 32 The distributions of dilatational damage parameter at 15% overall tensile strain [(a) isotropic damage model (the isotropic damage parameter), (b) separate dilatational/deviatoric damage model with $\alpha = 0.1$, (c) with $\alpha = 0.99$ and (d) with $\alpha = 10.0$].

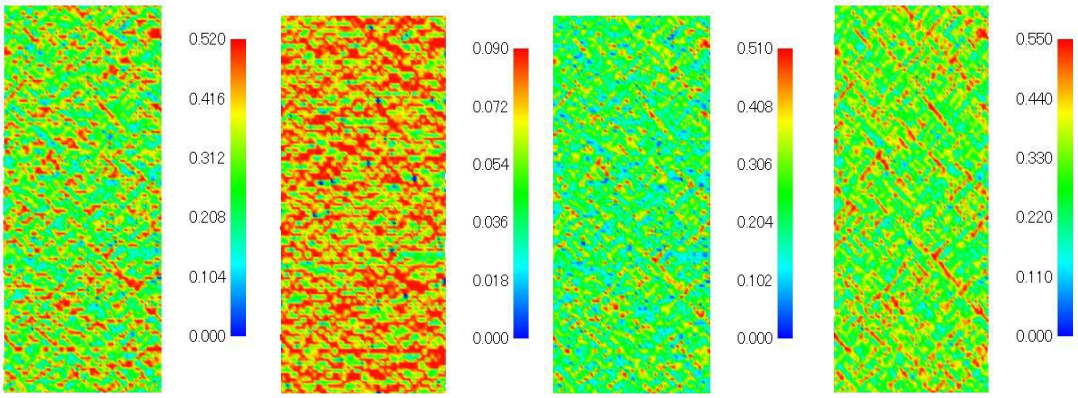

(a) Isotropic damage model (b) $\alpha = 0.1$ (c) $\alpha = 0.99$ (d) $\alpha = 10.0$

Figure 33 The distributions of deviatoric damage parameter at 15% overall tensile strain [(a) isotropic damage model (the isotropic damage parameter), (b) separate dilatational/deviatoric damage model with $\alpha = 0.1$, (c) with $\alpha = 0.99$ and (d) with $\alpha = 10.0$].

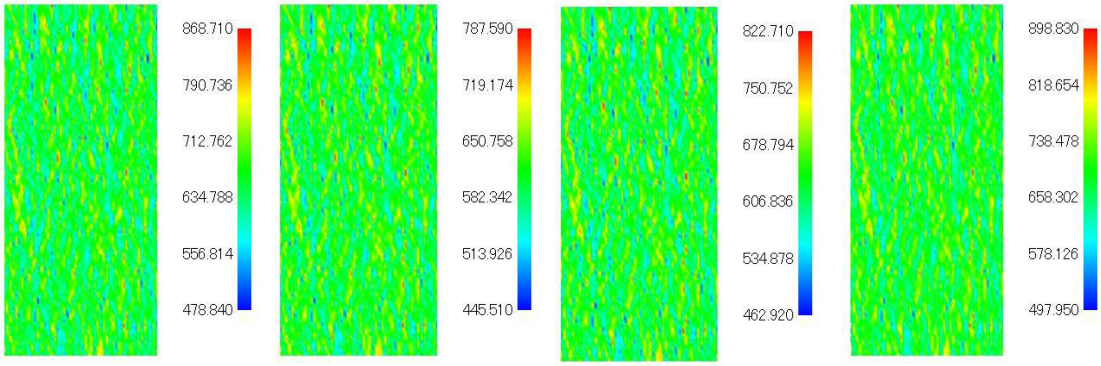

(a) Isotropic damage model (b) $\alpha = 0.1$ (c) $\alpha = 0.99$ (d) $\alpha = 10.0$

Figure 34 Tensile stress distributions at 10% overall tensile strain [(a) isotropic damage model, (b) separate dilatational/deviatoric damage model with $\alpha = 0.1$, (c) with $\alpha = 0.99$ and (d) with $\alpha = 10.0$].

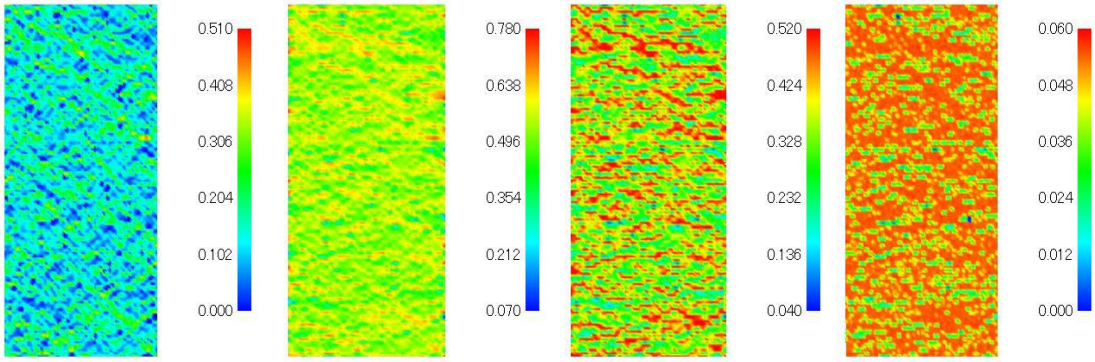

(a) Isotropic damage model (b) $\alpha = 0.1$ (c) $\alpha = 0.99$ (d) $\alpha = 10.0$

Figure 35 The distributions of dilatational damage parameter at 10% overall tensile strain [(a) isotropic damage model (the isotropic damage parameter), (b) separate dilatational/deviatoric damage model with $\alpha = 0.1$, (c) with $\alpha = 0.99$ and (d) with $\alpha = 10.0$].

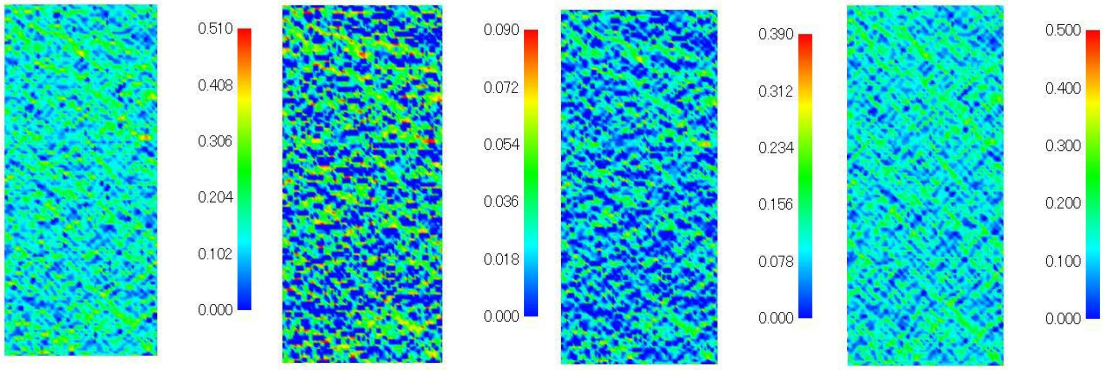

(a) Isotropic damage model (b) $\alpha = 0.1$ (c) $\alpha = 0.99$ (d) $\alpha = 10.0$

Figure 36 The distributions of deviatoric damage parameter at 10% overall tensile strain [(a) isotropic damage model (the isotropic damage parameter), (b) separate dilatational/deviatoric damage model with $\alpha = 0.1$, (c) with $\alpha = 0.99$ and (d) with $\alpha = 10.0$].

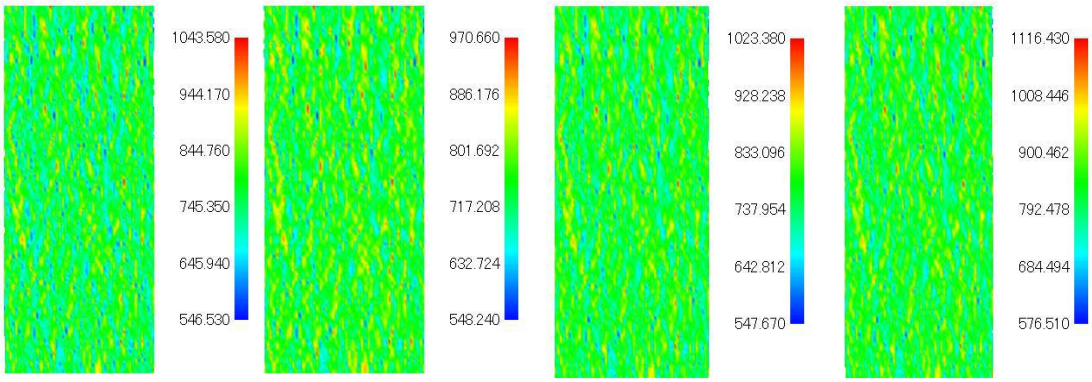

(a) Isotropic damage model (b) $\alpha = 0.1$ (c) $\alpha = 0.99$ (d) $\alpha = 10.0$

Figure 37 Tensile stress distributions at 15% overall tensile strain [(a) isotropic damage model, (b) separate dilatational/deviatoric damage model with $\alpha = 0.1$, (c) with $\alpha = 0.99$ and (d) with $\alpha = 10.0$].

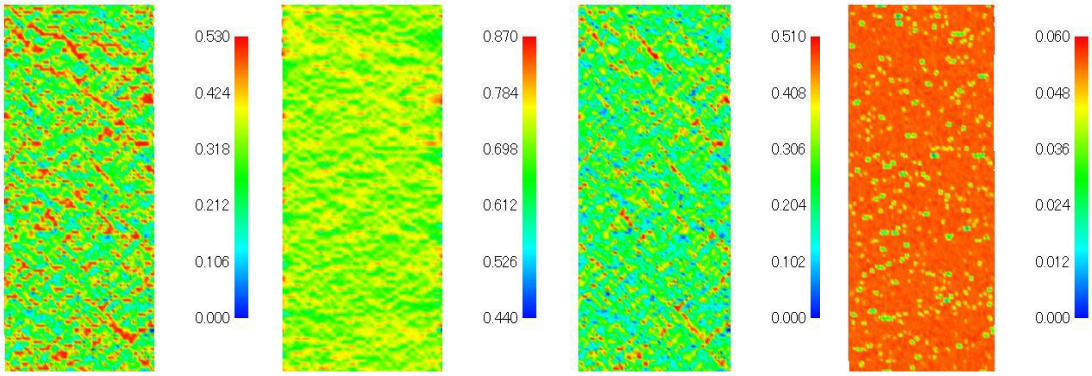

(a) Isotropic damage model (b) $\alpha = 0.1$ (c) $\alpha = 0.99$ (d) $\alpha = 10.0$

Figure 38 The distributions of dilatational damage parameter at 15% overall tensile strain [(a) isotropic damage model (the isotropic damage parameter), (b) separate dilatational/deviatoric damage model with $\alpha = 0.1$, (c) with $\alpha = 0.99$ and (d) with $\alpha = 10.0$.]

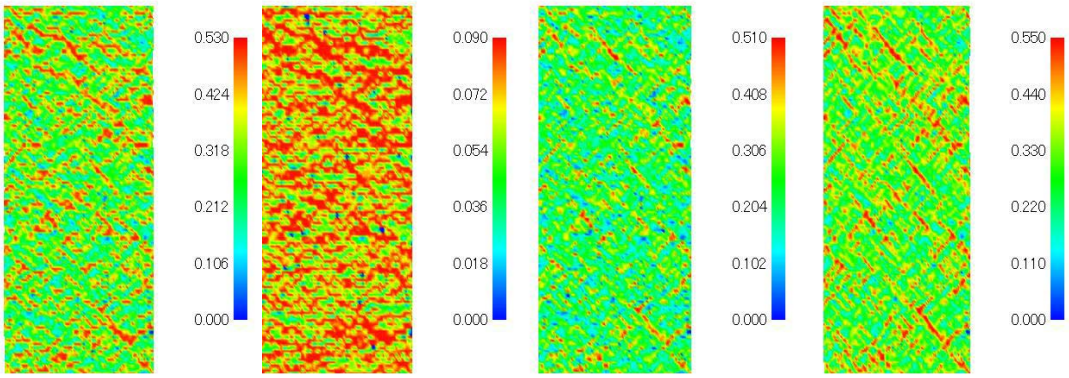

(a) Isotropic damage model (b) $\alpha = 0.1$ (c) $\alpha = 0.99$ (d) $\alpha = 10.0$

Figure 39 The distributions of deviatoric damage parameter at 15% overall tensile strain [(a) isotropic damage model (the isotropic damage parameter), (b) separate dilatational/deviatoric damage model with $\alpha = 0.1$, (c) with $\alpha = 0.99$ and (d) with $\alpha = 10.0$].

4.3 The behavior of a cracked specimen – isotropic damage model

In this section, we present results for cracked specimen. Finite element model is shown in Figure 21. Very fine meshes are placed at the vicinity of the crack tip and relatively small meshes are distributed throughout the analysis domain unlike the cases of ordinary crack analyses. In present analysis, we assume the spatial distribution of material stiffness and therefore it must be represented by the fine mesh discretization.

The distributions of material stiffness are assumed as shown in Figure 20.

The distributions of tensile stress for the material distribution models #1 and #2 and for homogeneous material case are shown in Figures 40 (a), (b) and (c), respectively, when the cracked blocks are subject to 0.3 % of overall tensile strain. In this loading step, entire analysis region has not undergone any nonlinear deformation. For the cases, in which the material distributions are assumed, we can see that there are the bands of relatively high stress regions running in vertical direction. In Figures 41 (a), (b) and (c) and 42 (a), (b) and (c), the distributions of tensile stress are presented for 5% and 7.5 % of overall strain, respectively. The bands of relatively high stress are seen in Figures 41 (a) and (b) and 42 (a) and (b). Other than these points, we do not see much difference between the distributed material stiffness models and the homogeneous model. In Figure 43, the distributions of the damage parameter are presented for 5% of overall strain. It is seen in Figures 43 (a) and (b) that damage zones develop at the crack tip and their shapes seem to be influenced by the material stiffness distributions. When the material is assumed to be homogeneous (Figure 43 (c)), the value of damage parameter gradually decreases as distance from the crack tip increases. In the cases of the distributed material stiffness models, the distributions of the damage parameter are more complex. We can see that, apart from the crack tip damage region, there are some scattered spots with relatively large value of the damage parameter. The shapes of crack tip damage regions are influenced by the distributed material stiffness. In Figure 44, the distributions of the damage parameter are shown for overall strain 7.5%. In the cases of the distributed material stiffness models, there are many scattered spots having large values of the damage parameter. The shapes of crack tip damage zones are somewhat irregular.

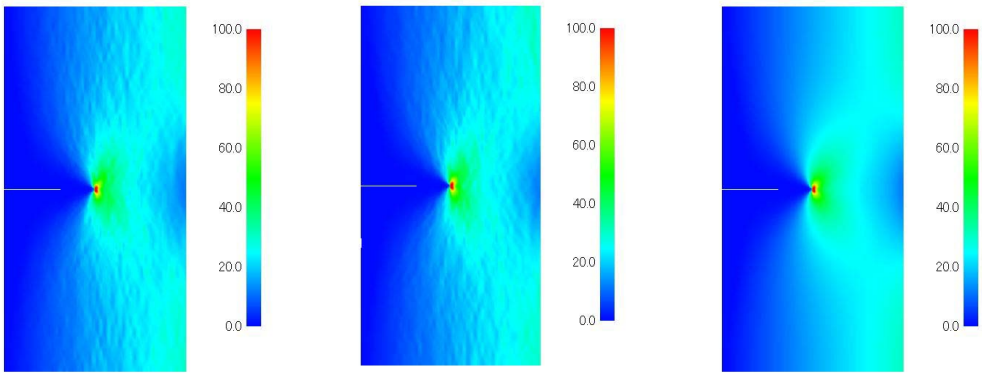

(a) Model #1 (b) Model #2 (c) Homogeneous

Figure 40 Tensile stress distributions at overall tensile strain 0.3% for (a) the distributed material stiffness model #1, (b) model #2 and (c) homogeneous material, with the isotropic damage constitutive model.

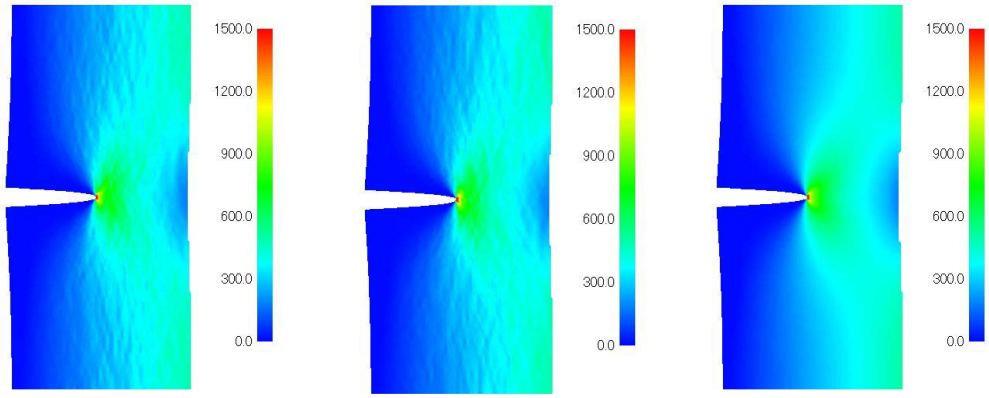

(a) Model #1 (b) Model #2 (c) Homogeneous

Figure 41 Tensile stress distributions at overall tensile strain 5% for (a) the distributed material stiffness model #1, (b) model #2 and (c) homogeneous material, with the isotropic damage constitutive model.

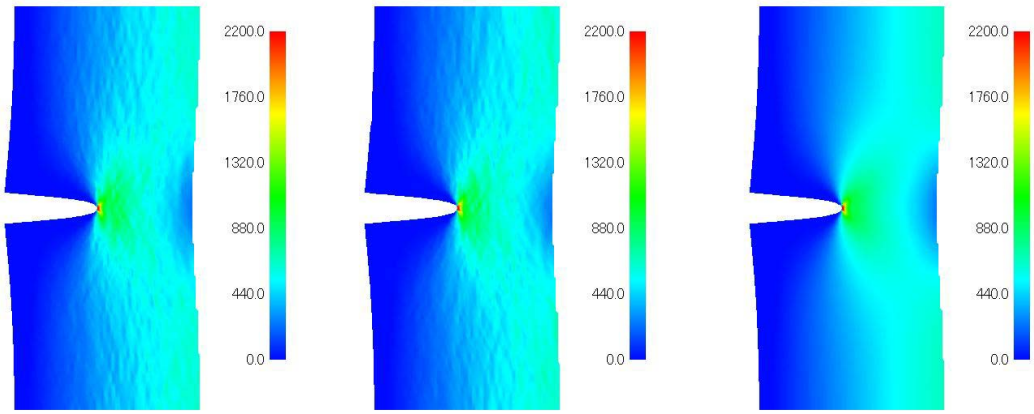

(a) Model #1 (b) Model #2 (c) Homogeneous

Figure 42 Tensile stress distributions at overall tensile strain 7.5% for (a) the distributed material stiffness model #1, (b) model #2 and (c) homogeneous material, with the isotropic damage constitutive model.

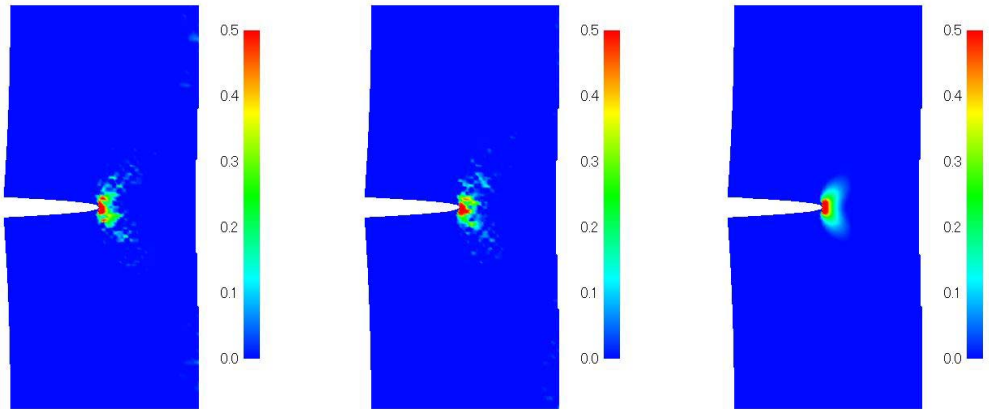

(a) Model #1 (b) Model #2 (c) Homogeneous

Figure 43 The distributions of the damage parameter at overall tensile strain 5% for (a) the distributed material stiffness model #1, (b) model #2 and (c) homogeneous material, with the isotropic damage constitutive model.

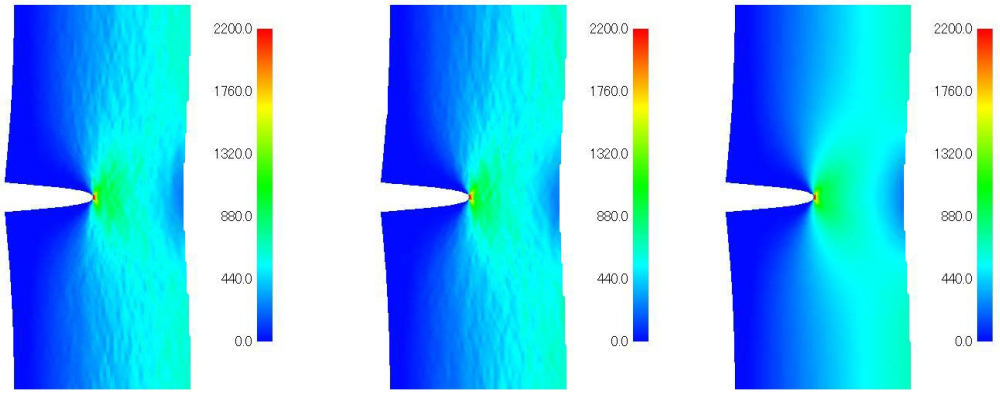

(a) Model #1 (b) Model #2 (c) Homogeneous

Figure 44 The distributions of the damage parameter at overall tensile strain 7.5% for (a) the distributed material stiffness model #1, (b) model #2 and (c) homogeneous material, with the isotropic damage constitutive model.

4.4 The behavior of a cracked specimen – separate isotropic/deviatoric damage model

In this section, the results of the separate isotropic/deviatoric damage model for the cracked block subject to tensile deformation are described. The constant α which controls the damage mode (volumetric, deviatoric or both of them) is set to be 0.1, 0.99 or 10.0.

In Figure 45, the distributions of tensile stress are presented for the distributed material stiffness model #1 when the cracked block is subject to 5% of tensile deformation. Figures 45 (a), (b), (c) and (d) show the results of the isotropic damage model and the separate isotropic/deviatoric damage model with $\alpha = 0.1$, $\alpha = 0.99$ and $\alpha = 10.0$, respectively. For all the material models, we do not find much difference.

In Figure 46, the distributions of the volumetric damage parameter are presented. For a comparison purpose, the result for the isotropic damage model is also shown in Figure 46 (a). In Figures 46 (b), (c) and (d), the results for $\alpha = 0.1$, $\alpha = 0.99$ and $\alpha = 10.0$ are depicted, respectively. The shapes of crack tip volumetric damage regions are almost the same in Figures 46 (b), (c) and (d). Their levels are different as the constant α is set to be 0.1, 0.99 or 10.0. In Figure 47, the distributions of the deviatoric damage parameter are shown. For a comparison purpose, the result of the isotropic damage model is also

depicted. The shapes of crack tip damage zones are similar to each other, including the case of the isotropic model. However, it is seen that as the value of the constant α increases, the damage zone tends to extend to upward and downward directions. When α is set to be 10.0, the shape of the damage zone is similar to that of plastic zone of elastic-plastic analysis.

In Figure 48, the distributions of tensile stress are presented for 7% of overall strain. We do not find much difference between the cases of the isotropic model and the separate volumetric/deviatoric damage model with $\alpha = 0.1$, $\alpha = 0.99$ and $\alpha = 10.0$. In Figures 49 (b), (c) and (d), the distributions of the volumetric damage parameters are presented. The case of the isotropic damage is also depicted in Figure 49 (a), for a comparison purpose. The shapes of crack tip volumetric damage zones are almost the same. However, their levels are different from each other, as the values of the constant α are set to be 0.1, 0.99 and 10.0. In Figures 50 (b), (c) and (d), the distributions of the deviatoric damage parameter are depicted. The shapes of crack tip deviatoric damage zones in the cases of $\alpha = 0.99$ and $\alpha = 10.0$ are similar. The damage zones extend in upward and downward directions from the crack tip. In the case of $\alpha = 0.1$, the damage zone extends in the forward direction from the crack tip. However, the value of the damage parameter is very small compared with those of $\alpha = 0.99$ and $\alpha = 10.0$

In Figures 51-56, the results that were obtained by the distributed material stiffness model #2 are presented. We find the same observations as the case of the model #1.

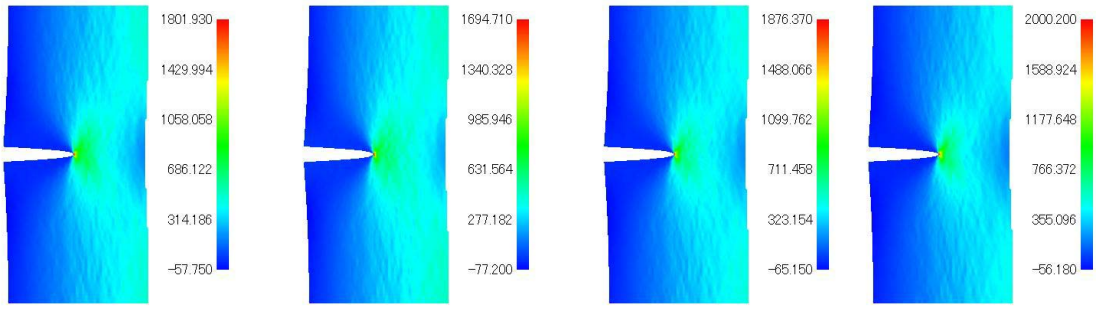

(a) Isotropic (b) $\alpha = 0.1$ (c) $\alpha = 0.99$ (d) $\alpha = 10.0$

Figure 45 Tensile stress distributions of crack model #1 at 5% overall tensile strain [(a) isotropic damage model, (b) separate dilatational/deviatoric damage model with $\alpha = 0.1$, (c) with $\alpha = 0.99$ and (d) with $\alpha = 10.0$].

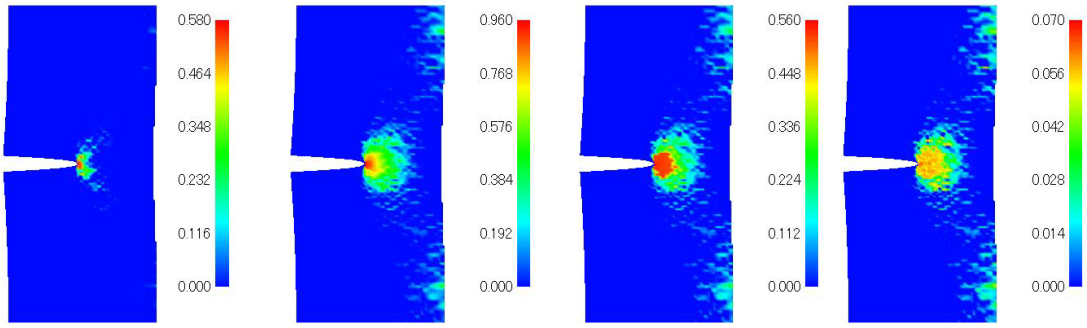

(a) Isotropic (b) $\alpha = 0.1$ (c) $\alpha = 0.99$ (d) $\alpha = 10.0$

Figure 46 The distributions of the volumetric damage parameter of crack model #1 at 5% overall tensile strain [(a) isotropic damage model (the isotropic damage parameter), (b) separate dilatational/deviatoric damage model with $\alpha = 0.1$, (c) with $\alpha = 0.99$ and (d) with $\alpha = 10.0$].

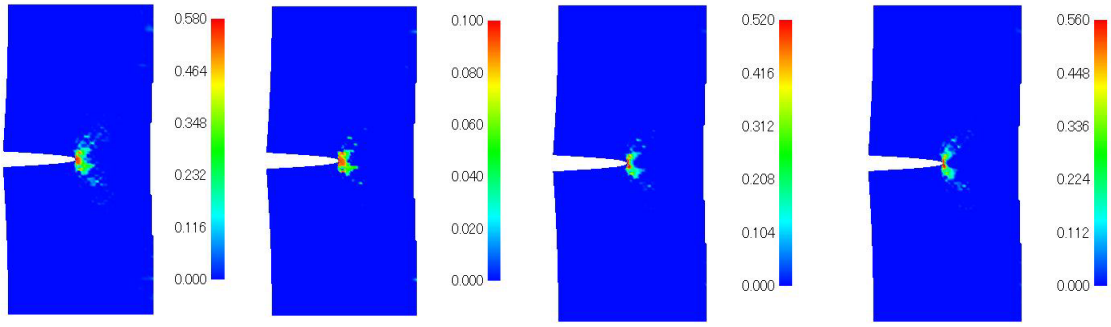

(a) Isotropic (b) $\alpha = 0.1$ (c) $\alpha = 0.99$ (d) $\alpha = 10.0$

Figure 47 The distributions of the deviatoric damage parameter of crack model #1 at 5% overall tensile strain [(a) isotropic damage model (the isotropic damage parameter), (b) separate dilatational/deviatoric damage model with $\alpha = 0.1$, (c) with $\alpha = 0.99$ and (d) with $\alpha = 10.0$].

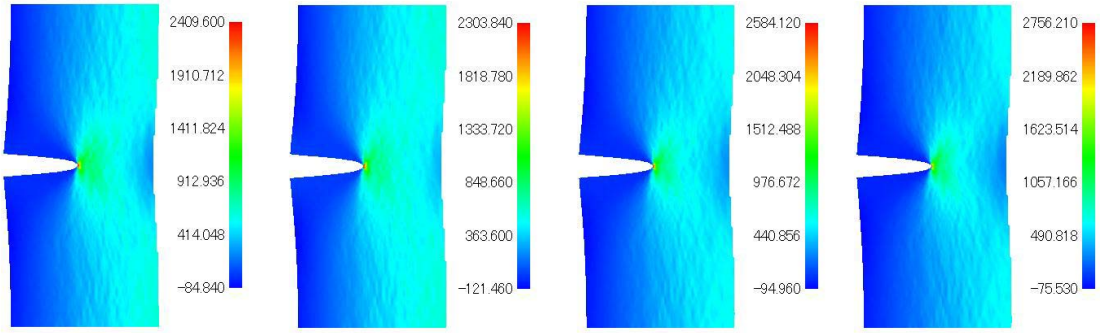

(a) Isotropic (b) $\alpha = 0.1$ (c) $\alpha = 0.99$ (d) $\alpha = 10.0$

Figure 48 Tensile stress distributions of crack model #1 at 7% overall tensile strain [(a) isotropic damage model, (b) separate dilatational/deviatoric damage model with $\alpha = 0.1$, (c) with $\alpha = 0.99$ and (d) with $\alpha = 10.0$].

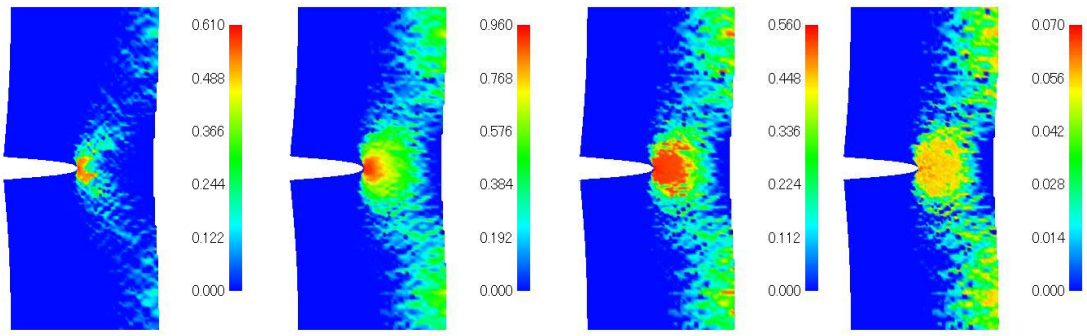

(a) Isotropic (b) $\alpha = 0.1$ (c) $\alpha = 0.99$ (d) $\alpha = 10.0$

Figure 49 The distributions of the volumetric damage parameter of crack model #1 at 7% overall tensile strain [(a) isotropic damage model (the isotropic damage parameter), (b) separate dilatational/deviatoric damage model with $\alpha = 0.1$, (c) with $\alpha = 0.99$ and (d) with $\alpha = 10.0$].

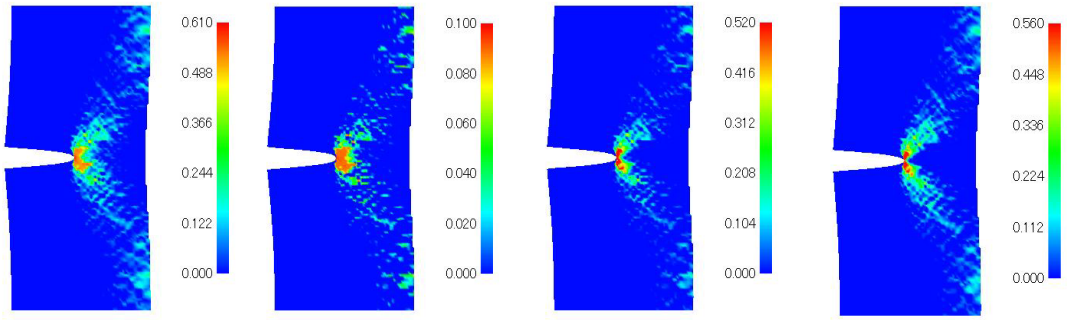

(a) Isotropic (b) $\alpha = 0.1$ (c) $\alpha = 0.99$ (d) $\alpha = 10.0$

Figure 50 The distributions of the deviatoric damage parameter of crack model #1 at 7% overall tensile strain [(a) isotropic damage model (the isotropic damage parameter), (b) separate dilatational/deviatoric damage model with $\alpha = 0.1$, (c) with $\alpha = 0.99$ and (d) with $\alpha = 10.0$].

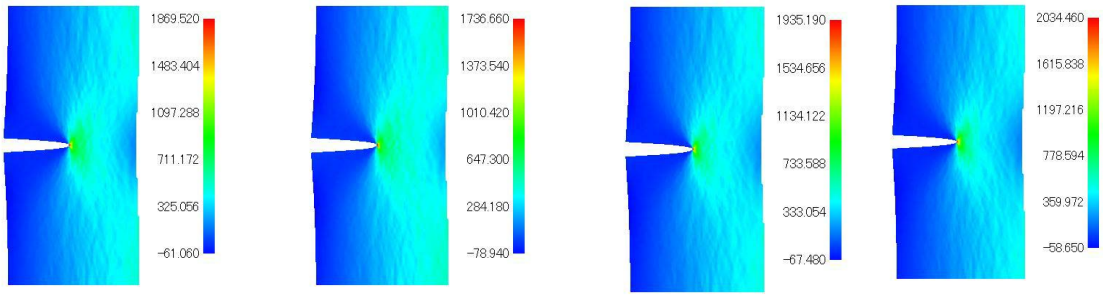

(a) Isotropic (b) $\alpha = 0.1$ (c) $\alpha = 0.99$ (d) $\alpha = 10.0$

Figure 51 Tensile stress distributions of crack model #2 at 5% overall tensile strain [(a) isotropic damage model, (b) separate dilatational/deviatoric damage model with $\alpha = 0.1$, (c) with $\alpha = 0.99$ and (d) with $\alpha = 10.0$].

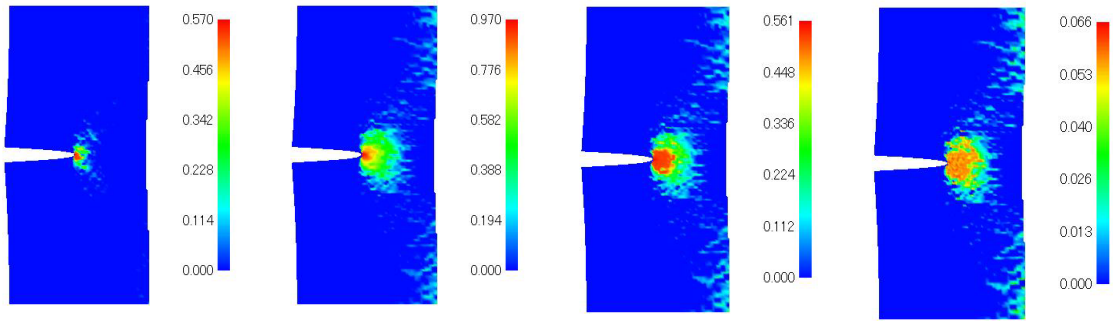

(a) Isotropic (b) $\alpha = 0.1$ (c) $\alpha = 0.99$ (d) $\alpha = 10.0$

Figure 52 The distributions of the volumetric damage parameter of crack model #2 at 5% overall tensile strain [(a) isotropic damage model (the isotropic damage parameter), (b) separate dilatational/deviatoric damage model with $\alpha = 0.1$, (c) with $\alpha = 0.99$ and (d) with $\alpha = 10.0$].

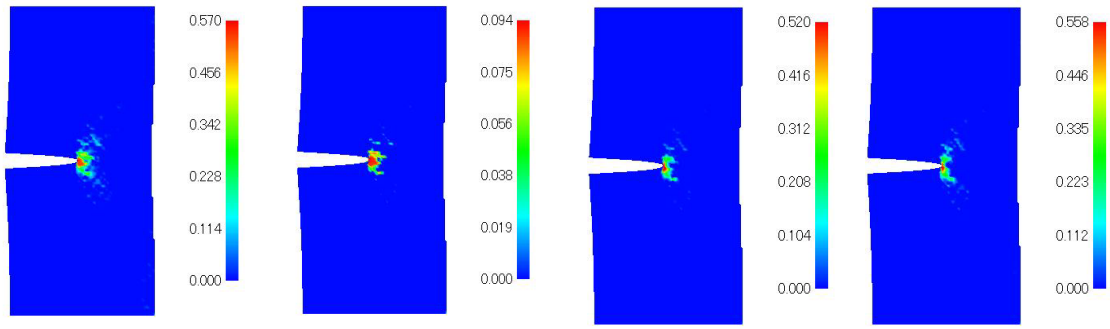

(a) Isotropic (b) $\alpha = 0.1$ (c) $\alpha = 0.99$ (d) $\alpha = 10.0$

Figure 53 The distributions of the deviatoric damage parameter of crack model #2 at 5% overall tensile strain [(a) isotropic damage model (the isotropic damage parameter), (b) separate dilatational/deviatoric damage model with $\alpha = 0.1$, (c) with $\alpha = 0.99$ and (d) with $\alpha = 10.0$].

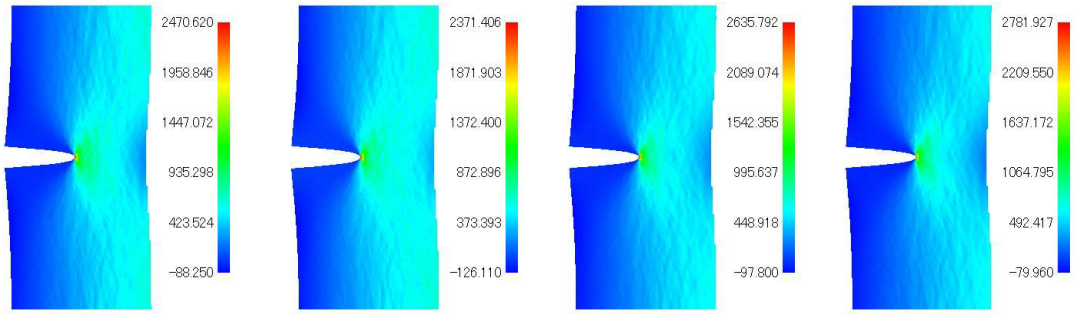

(a) Isotropic (b) $\alpha = 0.1$ (c) $\alpha = 0.99$ (d) $\alpha = 10.0$

Figure 54 Tensile stress distributions of crack model #2 at 7% overall tensile strain [(a) isotropic damage model, (b) separate dilatational/deviatoric damage model with $\alpha = 0.1$, (c) with $\alpha = 0.99$ and (d) with $\alpha = 10.0$].

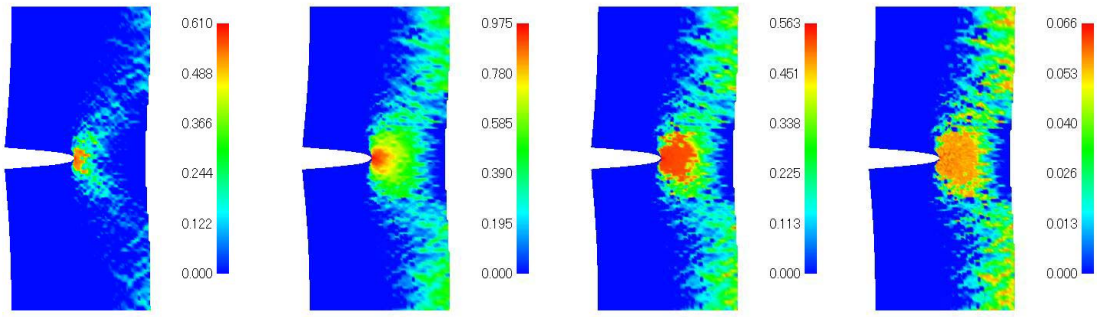

(a) Isotropic (b) $\alpha = 0.1$ (c) $\alpha = 0.99$ (d) $\alpha = 10.0$

Figure 55 The distributions of the volumetric damage parameter of crack model #2 at 7% overall tensile strain [(a) isotropic damage model (the isotropic damage parameter), (b) separate dilatational/deviatoric damage model with $\alpha = 0.1$, (c) with $\alpha = 0.99$ and (d) with $\alpha = 10.0$].

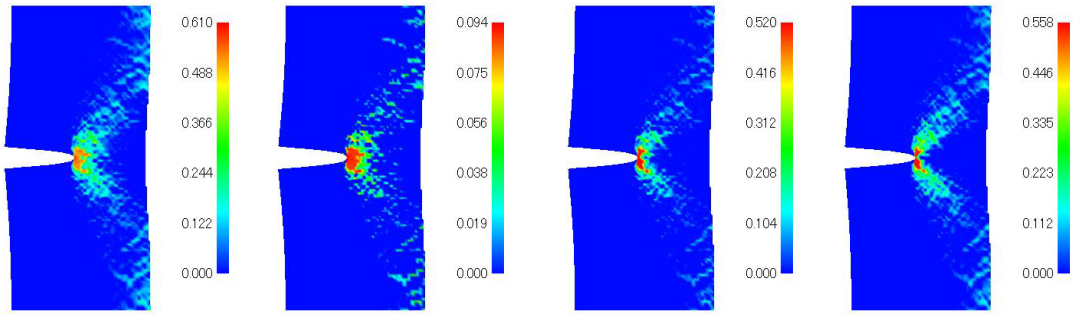

(a) Isotropic (b) $\alpha = 0.1$ (c) $\alpha = 0.99$ (d) $\alpha = 10.0$

Figure 56 The distributions of the deviatoric damage parameter of crack model #2 at 7% overall tensile strain [(a) isotropic damage model (the isotropic damage parameter), (b) separate dilatational/deviatoric damage model with $\alpha = 0.1$, (c) with $\alpha = 0.99$ and (d) with $\alpha = 10.0$].

5. Remarks

5.1 Summary of present investigation

In this report, the results of analyses in which material is assumed to be polymeric particulate composites and their spatial distributions are not homogeneous are presented. The uneven distributions of the particles are assumed to influence the stiffness of the material. The material undergoes damages due to dewetting between the particles and the polymeric matrix material and due to the growth of microvoids. They are accounted for by the damage models. In order to model the uneven distributions of the particles, we assumed the spatial distributions of overall material stiffness.

Two types of damage models were implemented in our in-house finite element computer program. One is the isotropic damage model and the other is the separate volumetric/deviatoric damage model. Both the constitutive models are based on the theory of Simo and Ju [1]. The separate volumetric/deviatoric model was developed during this course of study in order to model material damage due to the dilatational deformation of material. This damage mode is mainly due to the growth of microvoids and dewetting between the particles and matrix material.

Since the material properties of each material constituents were not known, we fitted the experimental one-dimensional stress-strain curve of Kwon and Liu [11] by the damage constitutive models. Detailed procedures to obtain relationships between the effective stress-like parameters and the damage parameters were developed.

The damage constitutive models (the isotropic and the separate volumetric/deviatoric damage constitutive models) were implemented in our in-house s-version finite element (s-FEM) program. The s-FEM computer program was used to perform the analyses of tensile block and that with a crack. The particles in the polymeric composites distribute unevenly at a local level but evenly at larger scale level. The distribution of the particles is statistically uniform but varies locally. Experimental evidences show that representative area of 2 mm x 2 mm is large enough so that the particle volume fractions of different 2 mm x 2 mm representative areas are almost the same. Thus, we built two different statistically the same distributed stiffness models. The variations of the stiffness of the material reflect the variations of particle volume fraction.

Finite element analyses were performed and the distributions of the tensile stress and the damage parameters were visualized.

5.2 Findings from the analyses

From the results of tension blocks, regions of high and low stresses connect in vertical direction. The distributions at the same overall strain are similar to each other except for the case of $\alpha = 10.0$ at 15% of overall strain. The differences in stress values at high and low locations are more pronounced in the case of $\alpha = 10.0$ at 15% of overall strain than the other case. It is considered that the distributions of the stress are governed by the spatial variation of material stiffness. However, the values are influenced by how the damage is sensitive to hydrostatic or deviatoric stress. That is why $\alpha = 10.0$, in which the material damage is much more sensitive to the deviatoric stress gives somewhat different result from the others.

The distributions of damage parameters give us very interesting insights. In all the cases, we find the bands of large values of the damage parameters. When the isotropic damage model is adopted, the bands tend to run in the direction 40~50 degrees from the loading axis. When the separate volumetric/deviatoric damage model is applied to the analyses, the bands of large value of the deviatoric damage parameter run in about 45 degree direction from the tensile axis and those of the volumetric damage parameter are perpendicular to the loading direction. This means that the bands of highly damaged regions are influenced not only by the spatial variation of material stiffness but also by the mode of damage. In the case of $\alpha = 10.0$ in which the deviatoric damage is considered to dominate the volumetric mode, the direction of maximum shear stress. When the volumetric damage mode dominates the other ($\alpha = 0.1$), the damage zones extend in the section of maximum tensile stress. It is considered that once a spot of damaged zone is present, it raises the tensile stress at the vicinity of the weakened spot in the direction perpendicular to the loading axis, as shown in Figure 57. Thus, the hydrostatic stress at that position enlarges, resulting in the progressive material damage. For the case of deviatoric damage, it is considered that the damage zones tend to have the 45 degree directions from the loading axis for the similar reason.

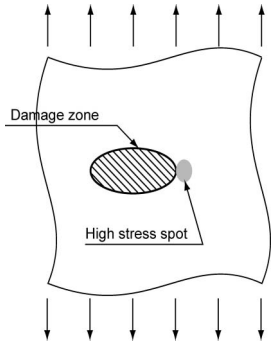

Figure 57 High stress spot adjacent to the damage zone

5.3 Relevance to the case of polymeric particulate composite

Though in this research, we have conducted an investigation on the damage behavior of continuum damage solids. The growth of microvoids is considered to be governed by the hydrostatic stress. Therefore, the volumetric damage mode takes the central role in such a case. When the dewetting between the particles and the polymeric matrix material is considered, the damage mechanisms may be more complex than the case of the growth of microvoids. However, after a particle is separated from matrix material completely, it behaves as a void. Therefore, the growth of voids plays a major role in the deformation mechanisms of the composite.

The contributions of deviatoric stress components to the material damage are not known. If the growth of microvoids and the dewetting of the particles were the major phenomena in the damage processes, we should use the separate volumetric/deviatoric damage model with small value of constant α.

6. Conclusions

In this investigation, we have used the damage constitutive models and the results of different models have been compared with each other. Blocks with and without a crack subject to tensile deformation were analyzed by the finite element method. The major findings are:

(1) Bands of highly damaged zones develop in the tensile block and their directions depend on the constitutive model. They have about 30, 45 and 90 degree directions when the isotropic and the separate volumetric/deviatoric damage model with the constant α being 10 and 0.1, respectively. The cases of $\alpha = 10.0$ and $\alpha = 0.1$ almost correspond to those of deviatoric and dilatational damage models, respectively.

(2) Two different statistically the same material stiffness variations in the tension blocks were assumed. The overall trends did not change as long as the distributions were statistically the same.

(3) The shapes of crack tip damage zones depend on the local variations of the material stiffness at the crack tip. However, the overall trends were the same for the same statistical distributions of material stiffness.

(4) The shapes of the crack tip damage zone depended on the constitutive models.

References

(1) J. C. Simo and J.W. Ju
Strain- and Stress Based Continuum Damage Models-I. Formulation, *Int. J. Solids Structures*, Vol. 23, pp. 821-840, 1987.
(2) J. C. Simo and J.W. Ju
Strain- and Stress Based Continuum Damage Models-II. Computational Aspects, *Int. J. Solids Structures*, Vol. 23, pp. 841-869, 1987.
(3) H. Okada, C. T. Liu, T. Ninomiya, Y. Fukui and N. Kumazawa
Analysis of Particulate Composite Materials using an Element Overlay Technique, *CMES: Compute Modeling in Engineering & Sciences*, Vol. 6, pp. 333-347, 2004.
(4) J. Fish
The s-Version Finite Element Method, *Computers & Structures*, Vol. 43, pp. 539-347, 1992.
(5) J. Fish and R. Guttal (1996)
The s-Version of Finite Element Method for Laminated Composites, *Int. J. Numer. Methods Eng.*, Vol. 39, pp. 3641-3662, 1996.
(6) S. Tanaka, H. Okada, Y. Watanabe and T. Wakatsuki
Applications of s-FEM to the Problems of Composite Materials with Initial Strain-Like Terms, *International Journal for Multiscale Computational Engineering*, to appear, 2006.
(7) H. Okada, S. Endoh and M. Kikuchi
On Fracture Analysis using an Element Overlay Technique, Engineering Fracture Mechanics, vol. 72, pp. 773-789, 2005.
(8) S. Nakasumi, K. Suzuki, D. Fujii and H. Ohtsubo
Mixed analysis of shell and solid elements using the overlaying mesh method, *Journal of Marine Science and Technology*, vol. 7, pp. 180-188, 2003.
(9) H. Okada, C. T. Liu, T. Ninomiya, Y. Fukui and N. Kumazawa,
Applications of Element Overlay Technique to the Problems of Particulate Composite Materials, ICCES'04 (International Conference on Computational and Experimental Mechanics), Edt. A Tadeu and S.N. Atluri, CD-ROM, 2004.
(10) T. Oguni, K. Murata, T. Miyoshi, J.J. Dongarra and H. Hasegawa
Software for matrix computations (Gyouretsu Keisan Software), Matuzen, Tokyo, Japan, 1991.
(11) Y. W. Kwon and C. T. Liu

Effect of Particle Distribution in Initial Cracks Forming from Notch Tips of Composites with Hard Particles Embedded in a Soft Matrix, *Composites Part B*, Vol. 32, pp. 199-208, 2001.

Publications

S. Tanaka, H. Okada, Y. Watanabe, T. Wakatsuki
Applications of s-FEM to the problems of composite materials with initial strain-like terms, submitted to International Journal for Multiscale Computational Engineering, 2005 (accepted for the publication).

S. Tanaka, H. Okada, Y. Watanabe
Application of s-version FEM to the mesoscopic analysis of Wavy Shape Memory Fiber/Plaster Smart Composite, WCCM (International Congress on Computational Mechanics) IV, CD-ROM, 2004.

H. Okada, C.T. Liu and S. Tanaka
Analysis of Damage Evolution of Particulate Composite Material using the s-version FEM, *Proceedings of* International Conference on Computational & Experimental Engineering and Sciences 2005 (ICCES'05) (Edt. by S.M. Sivakumar, M. Meher Prasad, B. Dattaguru, S. Narayanan, A.M. Rajendran, S.N. Atluri), CD-ROM, 2005.

H. Okada and Y. Kamimaru
BEM Analysis on Crack Tip Deformation Field of Rubber-Modified Epoxy Resin, Adhesive Layer *Proceedings of* International Conference on Computational & Experimental Engineering and Sciences 2005 (ICCES'05) (Edt. by S.M. Sivakumar, M. Meher Prasad, B. Dattaguru, S. Narayanan, A.M. Rajendran, S.N. Atluri), CD-ROM, 2005.

H. Okada, S. Tanaka, Y. Fukui and N. Kumazawa
Analyses of progressive damage and fracture of particulate composite materials using S-FEM technique, to be presented at ECF16 (16th European Conference on Fracture), 2006.

Acknowledgements

The investigator of present research would like to express sincere thanks to the support from Asian Office of Aerospace Research and Development (AOARD). The sincere gratitude is extended to Dr. Tae-Woo Park for his encouragements during course of study and to Dr. C.T. Liu (formerly with Air Force Research Laboratory) for his kind guidance and technical support. Without their support, it was not possible to perform present investigation.

Former and current graduate students at the Graduate School of Science and Engineering of Kagoshima University put a lot of efforts in developing computer codes, in performing computation and in visualizing the results. Many thanks are extended to them (Mrs. Y. Sakasegawa, T. Ninomiya, Y. Kamimaru, T. Kamibeppu, K. Sanada, K. Oya and S. Tanaka).